# Äspö Hard Rock Laboratory

**TRUE Block Scale continuation project**

**BS2B pretests**

**Crosshole interference, dilution and tracer tests, CPT-1–CPT-4**

Peter Andersson

Sofia Gröhn

Rune Nordqvist

Eva Wass

GEOSIGMA AB

September 2004

**SKB**

**Äspö Hard Rock Laboratory**

# Äspö Hard Rock Laboratory

## TRUE Block Scale continuation project

## BS2B pretests

## Crosshole interference, dilution and tracer tests, CPT-1–CPT-4

Peter Andersson

Sofia Gröhn

Rune Nordqvist

Eva Wass

GEOSIGMA AB

September 2004

# Foreword

The current study present the results of a series of pre-tests which preceded performance of a tracer test with radioactive sorbing tracers.

Following completion of this study a redefinition of one of the primary structures (Structure #25) has been made to the effect that it has been attributed being two separate background fractures rather than being one single determistic structure. In fact, the very results presented in this study is one of the cornerstones in this redefinition, showing that the two intercepts are not directly hydraulically connected, but rather connected by way of Structure #19.

Consequently, the background fracture formerly called Structure #25 in section KI0025F02:R2 is in subsequent work referred to as (background fracture) BG1. The latter section constitutes one of the designated injection points for the planned tests with radioactive sorbing tracers. The corresponding second intercept of the former Structure #25, as interpreted in Section KI0025F03:R2, is degraded to simply being one of many anonymous background fractures. The latter section is not used in the planned tests with radioactive sorbing tracer tests

# Abstract

This report describes the performance and results of a series of pre-tests in the TRUE Block Scale Continuation Project (BS2B). The pre-tests have included a combination of flow and pressure interference tests and tracer tests with non-sorbing tracers. The main objective of the tests is to obtain a test geometry optimised for radioactive sorbing tracer tests planned within the project. The tests also aim to improve the hydro-structural model of the TRUE Block Scale site, in particular in the area of Structure #19 which has not been subject to tracer tests in the past. The tests involved six different test set-ups, the three first (CPT-1 to CPT-3) comprised tracer dilution tests combined with pumping and the three last (CPT-4a to CPT-4c) included multiple-hole tracer tests. The test results made it possible to identify two suitable candidates for tests with sorbing tracers, one being a flow path within the previously identified Structure #19 and the other being a minor "background fracture" connected to Structure #19.

# Sammanfattning

Denna rapport behandlar utförandet och resultaten av en serie hydrauliska tester och spårförsök inom TRUE Block Scale Continuation Project (BS2B). Testerna har omfattat tre stycken kombinerade flödes- och tryckinterferenstester samt tre spårförsök med icke-sorberande ämnen. Huvudsyftet med testerna har varit att försöka hitta en optimal testgeometri för planerade spårförsök med radioaktiva sorberande spårämnen. Testerna syftar också till att förbättra den hydro-strukturella modellen over TRUE Block Scale-siten, speciellt runt Struktur #19, i vilken inga spårförsök gjorts tidigare. Testerna inkluderade sex olika försöksuppställningar. De tre första (CPT-1 till CPT-3) omfattade utspädningsmätningar kombinerade med pumpning och de tre senare (CPT-4a till CPT-4c) inkluderade flerhålsspårförsök. Testresultaten gjorde det möjligt att identifiera två lämpliga kandidater för kommande tester med sorberande spårämnen. Den ena är en flödesväg inom den tidigare identifierade Struktur #19 och den andra är en mindre, singular, så kallad "bakgrundsspricka" som skär Struktur #19.

# Executive summary

The strategy for the forthcoming tracer tests in the TRUE Block Scale Continuation Project (BS2B) focused on tracer tests over longer distances in Structure #19 and, if possible, also in minor fractures connected to, or sub-parallel to Structure #19. A pre-test programme was needed to find suitable injection points (flow paths) for the planned tracer tests with radioactive sorbing tracers. This report describes the results of the pre-test programme.

The main objective with the pre-tests was to obtain a test geometry optimised for radioactive sorbing tracer tests planned within the TRUE Block Scale Continuation Project. The tests also aimed to improve the hydro-structural model of the TRUE Block Scale site, in particular in the area of Structure #19 which has not been subject to tracer tests in the past.

The test sequence included a series of pressure interference tests combined with tracer dilution tests (CPT-1 through CPT-3) and finally, also tracer tests with non-sorbing tracers (CPT-4a, -4b and -4c. The specific objectives for CPT1-3 were:

- To find the best possible sink for the tests with sorbing tracers.

- To find a set of candidate injection points for the sorbing tracer tests.

By using the selected candidates, CPT-4a and -4b were performed with the specific objectives of:

- Assessing that the selected flow paths gave a tracer mass recovery of <80%.

- Assessing the tracer residence time for a non-reactive tracer

Finally, CPT-4c was performed with the main objective of assessing the mass recovery for the finally selected flow paths under slightly different boundary conditions than in CPT-4a and -4b.

The evaluation of the interference tests involved analysis of the pressure responses in the surrounding borehole array by preparation of pressure response diagrams for each test and a unified pressure response matrix for all tests. In addition, flow responses were monitored by repeating tracer dilution tests before and during pumping.

In general, the performed interference tests confirm the existing hydro-structural model (Winberg et al., 2002). The pressure interference tests CPT-1 to CPT-3, using Structure #19 as sink, show similar response patterns, with high and fast responses in sections interpreted to include Structure #19 and high but significantly slower responses in sections including Structure #25. The Structure #20-system (Structure #20, #21, #22, #23) respond lower and slower. There are only a few responses that do no follow the pattern described above, in particular the very good responses in sections KI0025F:R1

(Structure Z), KI0023B:P3, KI0025F:R3 and KI0025F03:R1. These responses indicate that other fractures connected to Structure #19 are present, possible splay fractures to Structure #19.

The determination of flow rates using the tracer dilution method shows distinct responses in many observation sections. Natural (ambient) flow rates vary by between 3-42 ml/h and stressed flow rates go up as high as 400 ml/h due to the pumping.

The general conclusion drawn from the results of the pressure interference tests and tracer dilution tests is that the TRUE Block Scale array consists of at least three well separated hydraulic units, Structure #19, Structure #25 and Structure #20. Section KI0025F03:R3 was judged to be the best sink for the tracer tests performed in CPT-4 due to good flow and pressure responses, central location and suitable distance.

Tests CPT-4a - CPT-4c were focused on tracer transport and were performed by establishing a radially converging flow field with a constant withdrawal rate in borehole section KI0025F03:R3 (Structure #19). The withdrawal rate was established by using the maximum sustainable flow (2.6 - 2.8 l/min). Non-sorbing and non-radioactive tracers (fluorescent dyes) were injected either as decaying pulses or by simultaneous injection of water creating a weak dipole flow field. Samples were automatically withdrawn both in the injection and withdrawal sections.

The tracer tests in CPT-4 show that Structure #19 and Structure #25 are interconnected However, the implementation of the new structure #25 is questionable as it seem to consist of two separate fractures, only being indirectly connected through Structure #19.

Based on the results of the CPT-4 experiments (and the limitation that injections can only be performed in flow paths where a recovery >80% has been proven from the permit from SSI), two different types of flow paths could be foreseen for tracer injection with sorbing tracers:

- Transport in a single structure (#19). The only potential flow path having a mass recovery of > 80% is KI0025F02:R3 → KI0025F03:R3.

- Tracer transport involving a single background fracture (#25) in contact with structure #19. The only flow path available for a tracer experiment addressing this type of transport is the KI0025F02:R2 → KI0025F03:R3 flow path. This flow path has also given a mass recovery of > 80%.

An evaluation of the nine different breakthrough curves from CPT- 4a-c has been made by performing parameter estimation using three basic one-dimensional models:

- Advection-dispersion model with a single transport pathway (AD-1)

- Advection-dispersion model with two separate transport pathways (AD-2)

- Advection-dispersion model with matrix diffusion and a single pathway (MD)

These models have been fitted to the experimental tracer breakthrough curves by non-linear least squares regression. It may be pointed out that all nine tests were single-tracer tests, i.e. no additional tracers were injected simultaneously. Thus, there are only limited possibilities to assess to what extent matrix diffusion processes have been significant during the tests and this was also not an objective for the tests.

The model fits are generally fairly good for all of the nine breakthrough curves. In most of the cases, the AD-1 model appears to be inadequate for explaining the later parts of the curves, while the AD-2 and MD models in those cases usually provide a better fit.

Generally, estimated values are within typical ranges what may be expected for tracer tests on this scale. In only a few cases, parameter values appear to be unreasonably large or small. Estimated values of the tracer residence time range between about ten hours, for the faster transport pathways, to several hundreds of hours for the slower pathways. The estimated values of the dispersivity are typically in the range of a few metres, except for some of the pathways from fits with the AD-2 model. The parameter $A$ may be regarded as an approximate measure of the "effect" of matrix diffusion. This parameter is a composite measure of several more basic properties, such as rock porosity, diffusivity, etc. In order to make any conclusions about the basic properties contained in the $A$ parameter, additional data would be required. The estimated values of $A$ are consistent with typical ones obtained from other experiments in fractured crystalline rock (Moreno et al, 1983, Andersson et al, 2002).

# Contents

# 1    Introduction

## 1.1    Background

A programme has been defined to increase the understanding of the processes that govern retention of radionuclides transported in crystalline rock, the Tracer Retention Understanding Experiments (TRUE). The basic idea is to perform a series of tracer tests with progressively increasing complexity.

When the TRUE Programme was set up it was identified that the understanding of radionuclide transport and retention in the Block Scale (10-100 m) also required attention in terms of a separate experiment.  The TRUE Block Scale project was then initiated as an international partnership funded by ANDRA, ENRESA, Nirex, POSIVA, JNC and SKB (Winberg, 1997). The first phase of the TRUE Block Scale Project was finalised during 2002 in the Evaluation and Reporting Stage (Andersson et al, 2002a, b; Poteri et al., 2002; Winberg et al., 2002).

At the TRUE Block Scale TC #2 meeting in Stockholm, April 29th, 2003 a strategy for the forthcoming tracer tests in the TRUE Block Scale Continuation Project was discussed. The strategy focused on tracer tests over longer distances in Structure #19 and, if possible also in minor fractures connected to, or sub-parallel to Structure #19. The meeting concluded that two of the boreholes piezometers, KI0025F02 and KI0025F03, required optimisation to better focus on Structure #19. The meeting also concluded that a pre-test programme was needed to find suitable injection points (flow paths) for the planned tracer tests with radioactive sorbing tracers. The results of the latter programme are presented in this report.

## 1.2    Objectives

The main objective with the pre-tests is to obtain a test geometry optimised for radioactive sorbing tracer tests planned within the TRUE Block Scale Continuation Project. The tests also aim to improve the hydro-structural model of the TRUE Block Scale site, in particular in the area of Structure #19 which has not been subject to tracer tests in the past.

The test sequence includes a series of pressure interference tests combined with tracer dilution tests (CPT-1 through CPT-3) and finally, also tracer tests with non-sorbing tracers (CPT-4a, -4b and -4c. The specific objectives for CPT1-3 were:

- To find the best possible sink for the tests with sorbing tracers.

- To find a set of candidate injection points for the sorbing tracer tests.

By using the selected candidates, CPT-4a and -4b were performed with the specific objectives of:

- Assessing that the selected flow paths gave a tracer mass recovery of <80%.

- Assessing the tracer residence time for a non-reactive tracer

Finally, CPT-4c was performed with the main objective of assessing the mass recovery for the finally selected flow paths under slightly different boundary conditions than in CPT-4a and -4b.

# 2 Performance and evaluation procedure

## 2.1 Equipment and tracers used

The five characterisation boreholes involved in the TRUE Block Scale Project are instrumented with 6-11 inflatable packers isolating 5-10 borehole sections each. Two of the boreholes (KI0025F02 and KI0025F03) were re-instrumented before test start of the pre-tests to better isolate the selected target Structure #19. All isolated borehole sections are connected to the HMS-system through data loggers (Datascan). The sections planned to be used for tracer tests are equipped with three nylon hoses, two with an inner diameter of 4 mm and one with an inner diameter of 2 mm. The two 4-mm hoses are used for injection, sampling and circulation in the borehole section whereas the 2-mm hose is used for pressure monitoring.

The tracer dilution tests were performed using four identical equipment set-ups for tracer tests, i.e. allowing four sections to be measured simultaneously. A schematic drawing of the tracer test equipment is shown in Figure 2-1. The basic idea is to have an internal circulation in the borehole section. The circulation makes it possible to obtain a homogeneous tracer concentration in the borehole section and to sample the tracer concentration outside the borehole in order to monitor the tracer injection rate with time, and also the dilution rate.

Circulation is controlled by a pump with variable speed (A) and measured by a flow meter (B). Water and tracer injections are made with two different HPLC plunger pumps (C1 and C2) and sampling is made by continuously extracting a small volume of water from the system through a flow controller (constant leak) to a fractional sampler (D). Water and tracer solution is stored in two separate pressurised vessels (E1 and E2) under nitrogen atmosphere. The tracer test equipment has earlier been used in the TRUE Block Scale and TRUE-1 tracer tests (e.g. Andersson et al., 2002b).

The tracers used were three fluorescent dye tracers, Uranine (Sodium Fluorescein) from KEBO (purum quality), Amino G Acid from Aldrich (techn. quality) and Rhodamine WT from Holiday Dyes Inc. (techn. quality). These tracers have all been used extensively in the TRUE-1 and TRUE Block Scale tracer tests (Andersson et al., 2002b).
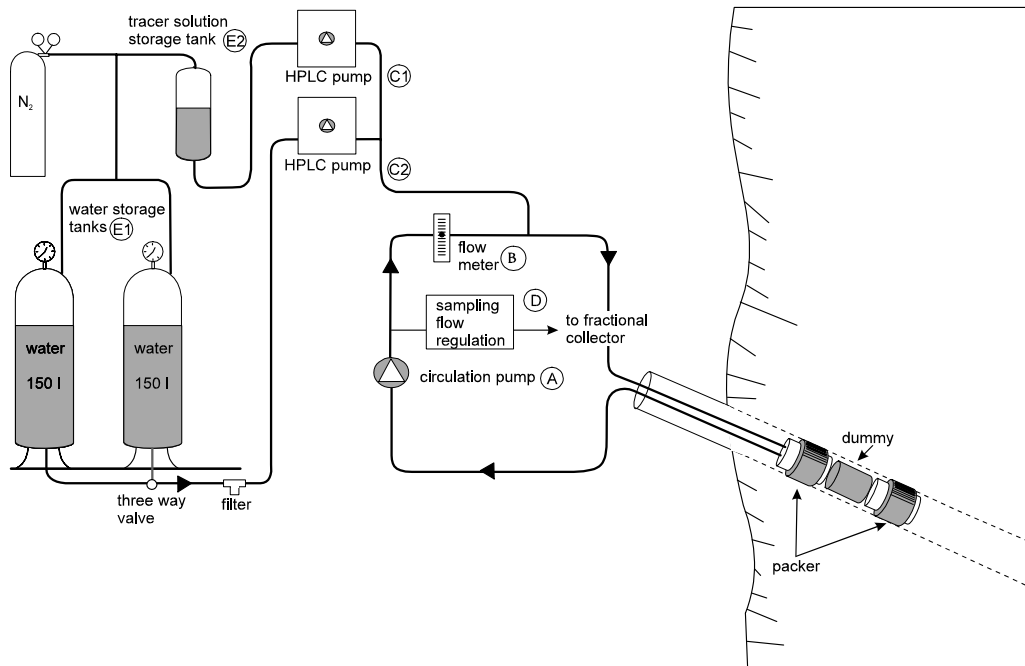
*Figure 2-1*. *Schematic drawing of the tracer injection/sampling system used in the TRUE Block Scale Continuation Project.*

## 2.2 Performance of the dilution tests, interference tests and tracer tests, CPT-1 - CPT-4

The TRUE Block Scale Continuation pre-tests involved six different test set-ups, the three first (CPT-1 to CPT-3) comprised tracer dilution tests combined with pumping and the two last (CPT-4a to CPT-4c) included multiple-hole tracer tests.

### 2.2.1 CPT-1 – CPT-3

The test cycle for tests CPT-1 to CPT-3 is similar to the one used in the TRUE-1 Continuation pre-tests CX-1 to CX-3 (Andersson et al., 2002c) and in the TRUE Block Scale pre-tests PT-1 to PT-4 (Andersson et al., 2001). Each test (CPT-1 - CPT-3) included measurements in 8 borehole sections and had a test cycle of four days with a pumping period of 48 hours. The test cycle comprised:

Day 1 - start tracer dilution test under ambient gradient in sections 1-4

Day 2 - start pumping in selected sink section, tracer dilution test under pumped conditions in sections 1-4

Day 3 - change of test sections to three new locations (sections 5-8), tracer dilution tests under pumped conditions

Day 4 – stop of pumping, tracer dilution test under ambient gradient, sections 5-8

The withdrawal flow was established using the maximum sustainable flow rate. The dimension of the tubing and the transmissivity of the section restricted the flow.

The pumping and recovery phases were performed as conventional constant rate pressure interference tests, implying that the flow rates and pressures were monitored with a high measurement frequency by the Äspö Hydro Monitoring System (HMS). Flow data from the sink section and the electrical conductivity of the withdrawal water were measured manually during the pumping phase after 1, 5, 10, 20, 30, 60 minutes of pumping and at regular intervals thereafter.

### 2.2.2 CPT-4a – CPT-4c

Tests CPT-4a - CPT-4c were focused on tracer transport and were performed by establishing a radially converging flow field with a constant withdrawal rate in borehole section KI0025F03:R3 (Structure #19). The withdrawal rate was established by using the maximum sustainable flow (2.6 - 2.8 l/min).

Non-sorbing and non-radioactive tracers (fluorescent dyes) were injected either as decaying pulses or by simultaneous injection of water creating a weak dipole flow field. Samples were automatically withdrawn both in the injection and withdrawal sections using techniques and equipment earlier developed in the TRUE Block Scale Project (Andersson et al., 2002b).

The first tracer test (CPT-4a) included three injections with the decaying pulse technique, i.e. without applying any excess pressure. This procedure introduced some tailing in the breakthrough curve due to the relatively slow decay of the input concentration. To remove some of this tailing effect, the injection of tracer solution was terminated by exchanging the tracer solution with unlabelled water soon after breakthrough was noted in the withdrawal section.

Since no excess pressure was applied in CPT-4a, the dilution rate in the injection sections was low and resulted in up to 25% of the tracer mass remaining in the injection sections after several hundreds of hours. This high concentration of tracer in the injection section after such a long time is disadvantageous from a safety aspect when handling radioactive tracers as planned for the sorbing tracer tests. It was therefore decided to repeat some of the pre-tests with an added injection flow rate of 5 ml/min (unlabelled formation water) and to make sure that the recovery did not decrease under these changed conditions.

The tracers used were Uranine (Sodium fluorescein), Rhodamine WT and Amino G Acid with injection concentrations in the order of 500-2000 ppm, cf. Chapter 3.6.

Additional parameters monitored were:

- pressure and hydraulic head (Äspö Hydro Monitoring System)

- withdrawal rate (manual measurements)

- electrical conductivity of withdrawn water (manual measurements)

Table 2-1 summarises the test set-ups including the sources and sinks used in the tests. Locations of the boreholes in the TRUE Block Scale array are shown in Figure *2-2* together with the main interpreted deterministic structures in the investigated rock volume.
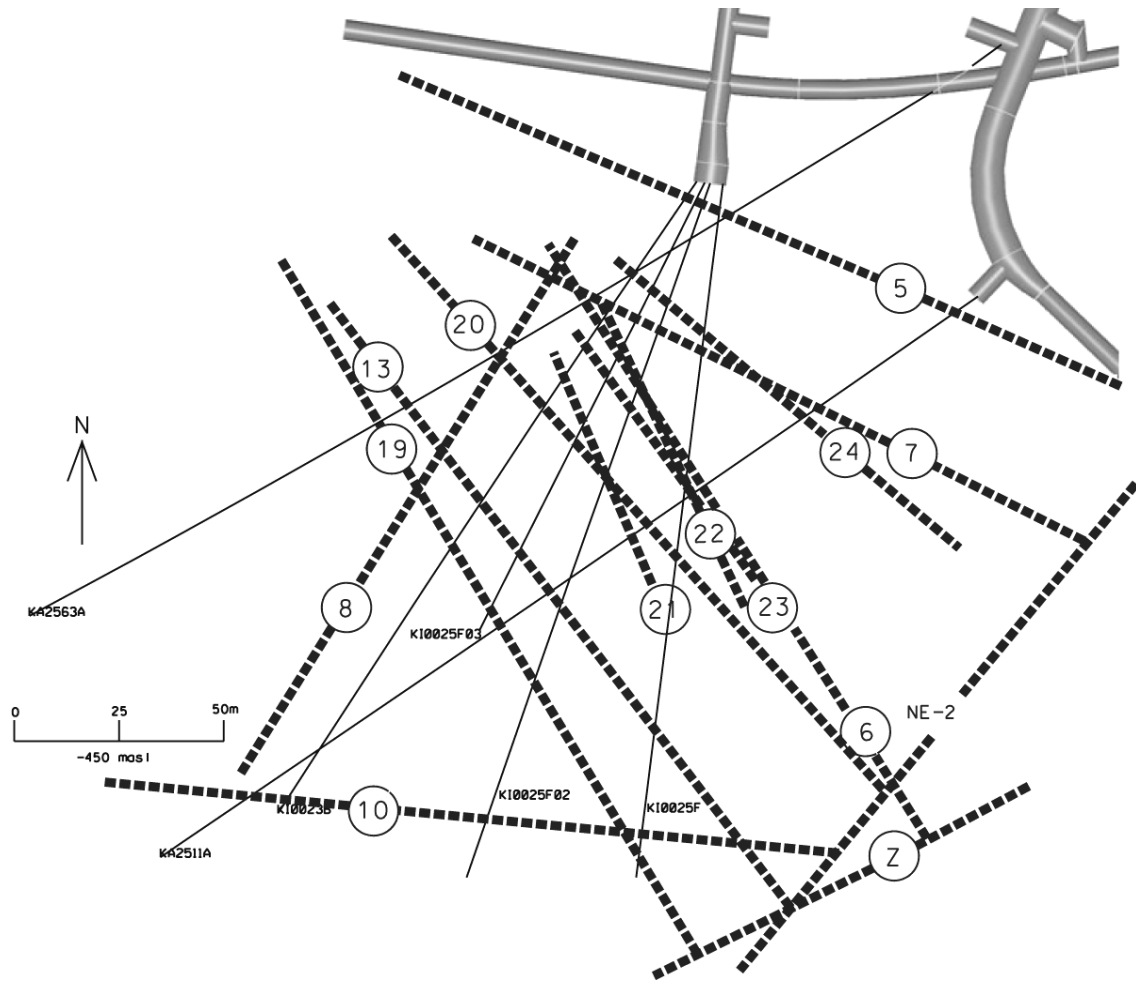
**Figure 2-2** *Horizontal section at Z=–450 masl (meters above sea level) showing structural model based on identified conductive geological structures in the TRUE Block Scale rock volume (Andersson et al. 2002b).*

**Table 2-1. Sources and sinks used for the pre-tests of the TRUE Block Scale Continuation. The borehole interval limits are given in Table 3-2.**

| Test | Sink | Structure | Source | Structure | Comment |
|------|------|-----------|--------|-----------|---------|
| CPT-1 | KI0025F:R2 | #19 | KI0025F02:R3 | #19 | Tracer dilution/interference test |
| | | | KI0025F03:R3 | #19 | |
| | | | KI0023B:P2 | #19 | |
| | | | KA2563A:S1 | #19 | |
| | | | KI0025F02:R2 | #25 | |
| | | | KI0025F03:R2 | #25 | |
| | | | KI0025F02:R5 | #13,21 | |
| CPT-2 | KI0025F02:R3 | #19 | KI0025F:R2 | #19 | Tracer dilution/interference test |
| | | | KI0025F03:R3 | #19 | |
| | | | KI0023B:P2 | #19 | |
| | | | KA2563A:S1 | #19 | |
| | | | KI0025F02:R2 | #25 | |
| | | | KI0025F03:R2 | #25 | |
| | | | KI0025F03:R5 | #13 | |
| | | | KI0025F02:R5 | #13,21 | |
| CPT-3 | KI0025F03:R3 | #19 | KI0025F:R2 | #19 | Tracer dilution/interference test |
| | | | KI0025F02:R3 | #19 | |
| | | | KI0023B:P2 | #19 | |
| | | | KA2563A:S1 | #19 | |
| | | | KI0025F02:R2 | #25 | |
| | | | KI0025F03:R2 | #25 | |
| | | | KI0025F03:R5 | #13 | |
| | | | KI0025F02:R5 | 13,21 | Contaminated |
| CPT-4a | KI0025F03:R3 | #19 | KI0025F:R2 | #19 | Tracer test (radially converging) |
| | | | KI0025F02:R3 | #19 | |
| | | | KI0023B:P2 | #19 | |
| CPT-4b | KI0025F03:R3 | #19 | KA2563A:S1 | #19 | Tracer test (weak dipole, rad conv.) |
| | | | KA2563A:S2 | #19 | |
| | | | KI0025F02:R2 | #25 | |
| CPT-4c | KI0025F03:R3 | #19 | KI0025F02:R3 | #19 | Tracer test (weak dipole) |
| | | | KI0023B:P2 | #19 | |
| | | | KI0025F02:R2 | #25 | |

## 2.3     Laboratory analyses

Samples were analysed for dye tracer content at the Geosigma Laboratory using a Jasco FP 777 Spectrofluorometer.

## 2.4     Evaluation

### 2.4.1     Hydraulic interference tests

The evaluation involves preparation of pressure response diagrams for each test and a unified pressure response matrix for all tests.

Time-drawdown (and recovery) plots were prepared for borehole sections showing a total drawdown of more than $s_p$=0.1 m (1 kPa) at stop of the flow period. This threshold drawdown was chosen with consideration of the amplitude of the tidal effects in the boreholes which may be in the order of 1-5 kPa. From these plots, the response times ($t_R$) for each section were estimated. The response time is here defined as the time after start of pumping when a drawdown (or recovery) of 1 kPa is observed (from the logarithmic plots) in the observation section. The qualitative evaluation has mainly been made on data from the drawdown phase. Data from the recovery phase were used only as supporting data.

On the X-axis of the pressure response diagrams (Figures 3-3, 3-7 and 3-10), the ratio of the response time ($t_R$) and the (squared) straight-line distance R between the (midpoint of) the sink section and (the midpoint of) each observation section ($t_R/R^2$) is plotted. The latter ratio is inversely related to the hydraulic diffusivity (T/S) of the rock, which indicates the speed of propagation in the rock of the drawdown created in the pumping section.

The final drawdown at stop of pumping ($s_p$) in the observation sections was determined from the drawdown data. To account for the different flow rates used in the tests and to make the pressure response plots comparable between tests, the final drawdown is normalised with respect to the final flow rate (Q). The ratio $s_p/Q$ is plotted on the Y-axis of the pressure response diagrams.

From the response plots of $s_p/Q$ versus $t_R/R^2$ for each test, sections with anomalous, fast response times (high hydraulic diffusivity) and large (normalised) drawdown can be identified. Such sections, showing primary responses, can be assumed to have a distinct hydraulic connection to the sink section and may be intersected by a single fracture; fracture zones or other conductive structures in the rock. Sections with delayed and weak (secondary) responses may correspond to sections in the rock mass between such structures.

From the calculated values of $s_p/Q$ (index 1) and $t_R/R^2$ (index 2) for each observation section during each test, a common pressure response matrix showing the response patterns for all tests, was prepared by classifying the pressure responses by means of the above indexes 1 and 2. For index 1, the following class limits and associated drawdown characteristics were used:

**Index 1 ($s_p/Q$)**

| | |
|---|---|
| $s_p/Q > 1 \cdot 10^5$ s/m$^2$ | Excellent (Red) |
| $3 \cdot 10^4 < s_p/Q \leq 1 \cdot 10^5$ s/m$^2$ | High (Yellow) |
| $1 \cdot 10^4 < s_p/Q \leq 3 \cdot 10^4$ s/m$^2$ | Medium (Green) |
| $s_p/Q \leq 1 \cdot 10^4$ s/m$^2$ | Low (Blue) |

For index 2 the following class limits and associated response characteristics were used:

**Index 2 ($t_R/R^2$)**

| | |
|---|---|
| $t_R/R^2 < 0.01$ s/m$^2$ | Excellent (E) |
| $0.01 \leq t_R/R^2 < 0.1$ s/m$^2$ | Good (G) |
| $0.1 \leq t_R/R^2 < 0.3$ s/m$^2$ | Medium (M) |
| $t_R/R^2 \geq 0.3$ s/m$^2$ | Bad (B) |

The results from the qualitative analysis of the hydraulic responses were compared with the hydro-structural model and the latter checked for consistency and possible need of revision. It should be pointed out that the response diagrams of $s_p/Q$ versus $t_R/R^2$ described above were only used as diagnostic tools to identify the most significant responses during each test and to construct the pressure response matrix. The diagrams should be used with some care since the true actual distances (along pathways) between the sink and observation sections are uncertain (particularly those involving $\geq 2$ structures), which may affect the position of a certain point (i.e. section) in the horizontal direction in the diagrams. However, in most cases, the shortest (straight-line) distance between the sink and observation section, as used here, is considered a sufficient and robust approximation for this purpose.

Another potential source of error in the response diagrams may occur if (internal) hydraulic interaction exists between sections along an observation borehole. For example, such interaction could either be due to packer leakage (insufficient packer sealing) or leakage in the rock through interconnected fractures around the packers. This situation may give rise to a false impression that good hydraulic communication exists between such observation sections and the actual source section. However, any analysis method will suffer from this potential source of error.

### 2.4.2   Tracer dilution tests

Flow rates were calculated from the decay of tracer concentration versus time through dilution with natural unlabelled groundwater, c.f. Andersson et al. (2002b). The so-called "dilution curves" were plotted as the natural logarithm of concentration versus time. Theoretically, a straight-line relationship exists between the natural logarithm of the relative tracer concentration ($c/c_0$) and time ($t$):

$$\ln (c/c_0) = - (Q_{bh} /V) \cdot \Delta t \qquad\qquad (2\text{-}1)$$

where $Q_{bh}$ (m$^3$/s) is the groundwater flow rate through the borehole section and $V$ (m$^3$) is the volume of the borehole section. By plotting $\ln (c/c_0)$ versus $t$, and by knowing the borehole volume $V$, $Q_{bh}$ may then be obtained from the slope of the straight line.

### 2.4.3   Tracer tests

#### *General*

In this report, an evaluation of the nine different breakthrough curves from CPT- 4a-c has been made by performing parameter estimation using three basic one-dimensional models:

- Advection-dispersion model with a single transport pathway

- Advection-dispersion model with two separate transport pathways

- Advection-dispersion model with matrix diffusion and a single pathway

These models have been fitted to the experimental tracer breakthrough curves by non-linear least squares regression. It may be pointed out that all nine tests were single-tracer tests, i.e. no additional tracers were injected simultaneously. Thus, there are only limited possibilities to assess to what extent matrix diffusion processes have been significant during the tests and this was also not an objective for the tests.

#### *Transport models*

*Advection dispersion model in a single pathway (AD-1)*

This model is described by the standard governing equation for one-dimensional advection-dispersion transport:

$$a_L v \frac{\partial^2 C}{\partial x^2} - v \frac{\partial C}{\partial x} = \frac{\partial C}{\partial t} \qquad\qquad (2\text{-}2)$$

where $C$ is concentration (e.q. M/L$^3$), $x$ is distance along transport path (L), $t$ is time (T), $v$ is the average water velocity (L/T) and $a_L$ is the longitudinal dispersivity (L).

The following initial and boundary conditions are applied:

$$C(x,t) = 0 \qquad\qquad t = 0 \tag{2-3}$$

$$\frac{\partial C(x,t)}{\partial x} = 0 \qquad\qquad x = \infty \tag{2-4}$$

$$-a_L v \frac{\partial C}{\partial x} + vC = C_0 \qquad\quad x = 0 \tag{2-5}$$

The above boundary and initial conditions results in a solution for a constant injection of tracer. For a tracer pulse with constant concentration of limited duration, the resulting tracer concentration may be calculated as:

$$C(x,t) = M(x,t) \qquad\qquad 0 < t \leq t_{inj} \tag{2-6}$$

$$C(x,t) = M(x,t) - M(x, t - t_{inj}) \qquad t > t_{inj} \tag{2-7}$$

where $M(x,t)$ is the solution for a step-input injection with constant injection concentration. A more complex temporal variation in the tracer injection may be calculated in an analogous way by summation of a several such injection periods. Solutions of the above equations are given, for example, Javandel et al (1984).

*Advection dispersion model in two pathways (AD-2)*

This model is essentially the same as the preceding one (AD-1) except that tracer transport is assumed to occur in two, or more, separate pathways and mix in the pumping section. This calculated by summing up the contribution from the different pathways as (for *n* pathways):

$$C(x,t) = \sum_{i=1}^{n} pf_i \cdot C_i(x,t) \tag{2-8}$$

where $C_i(x,t,)$ represents the partial tracer breakthrough from each individual pathway and *pf$_i$* is a proportionality factor that describes the contribution from each pathway.

It may here also be noted that the *pf* parameter also represents dilution effects in the pumping section as well as other proportional tracer losses. Thus, this parameter is often relevant to include also when applying the AD-1 model.

*Advection-dispersion model with matrix diffusion (one pathway)*

In this model, the governing equation for the AD model is extended by adding a term that represents diffusion of tracer into a hydraulically stagnant matrix:

$$\frac{\partial C}{\partial t} = -v\frac{\partial C}{\partial x} + a_L v\frac{\partial^2 C}{\partial x^2} + \frac{2 D_e}{\delta}\frac{\partial C_p}{\partial y} \qquad (2\text{-}9)$$

with the transport in the matrix given by:

$$\frac{\partial C_p}{\partial t} - \frac{D_e}{n_p}\frac{\partial^2 C_p}{\partial y^2} = 0 \qquad (2\text{-}10)$$

where $n_p$ is the matrix porosity, $D_e$ is the effective diffusion coefficient ($L^2$/T), $\delta$ is the fracture aperture (L) of the flowing fracture, $C_p$ $(y)$ is the tracer concentration in the matrix and $y$ is a spatial coordinate perpendicular to the direction of the flowing transport path. The matrix diffusion model used here is also presented by Tang et al. (1981) and Moreno et al. (1985).

When this matrix diffusion model is employed for interpretation of tracer breakthrough curves, all unknown parameters in equations 2-9 and 2-10 can not be evaluated independently. Instead, it is common to use a lumped parameter, *A*, which describes the effect of matrix diffusion. The parameter *A* may be written as:

$$A = \frac{\delta}{2\sqrt{n_p D_e}} \qquad (2\text{-}$$

11)With this definition, the matrix diffusion effect increases with decreasing values of *A*.

### Parameter estimation method

Estimated parameter values are obtained by non-linear least-squares regression. The basic non-linear least-squares regression minimises the sum of squared differences between the modelled ($Y^M$ ) and the observed ($Y^O$) variables and may be formulated as:

$$\text{Min S} = \mathbf{E_R}^T \mathbf{W} \mathbf{E_R} \qquad (2\text{-}12)$$

where $\mathbf{E_R}$ is a vector of residuals ($\mathbf{Y}^M - \mathbf{Y}^O$) and $\mathbf{W}$ is a vector of reliability weights on observations.

The specific method for carrying out the regression employed in this study is often referred to as the Marquardt-Levenberg method (Marquadt (1963), Levenberg (1944)). This method is a Newton-type optimisation algorithm that finds the parameter values that minimises the sum of squared errors between model and measurement values in an iterative manner. A simplified version of the search algorithm used may be written as:

$$\mathbf{B}_{r+1} = \mathbf{B}_r + (\mathbf{X}_r^T \mathbf{W} \mathbf{X}_r)^{-1} \mathbf{X}_r^T (\mathbf{Y}^O - \mathbf{Y}_r^M) \qquad (2\text{-}13)$$

where $\mathbf{B}$ is a vector of parameter estimates, $\mathbf{X}$ is a parameter sensitivity matrix, and the subscripts r and r+1 refer to the iteration number.

Given an initial parameter estimate, eq. (2-13) is repeated until a local optimal solution is found. The local minimum is defined by some convergence criterion, for example when parameter estimates are essentially identical between iterations. Finding a local minimum does not guarantee that the global minimum is found. When this appears to be a problem, several sets of initial estimates may be tried. When some knowledge about the parameters to be estimated and the physical system is already available, the initial estimates are often good enough for ensuring that a global minimum is found.

An important element of the above procedure is the matrix containing the parameter sensitivities. Parameter sensitivity is defined as the partial derivative of the dependent (simulated) variable with respect to a parameter. A sensitivity matrix contains one row for each observation and one column for each estimated parameter, as in the following example with three observations and two parameters.

$$\mathbf{X} = \begin{pmatrix} \dfrac{\partial y_1}{\partial b_1} & \dfrac{\partial y_1}{\partial b_2} \\ \dfrac{\partial y_2}{\partial b_1} & \dfrac{\partial y_2}{\partial b_2} \\ \dfrac{\partial y_3}{\partial b_1} & \dfrac{\partial y_3}{\partial b_2} \end{pmatrix} \tag{2-14}$$

Parameter sensitivities may be used to determine the precision of the estimated parameter values. Given below are two diagnostic measures regarding parameter uncertainty that may be obtained as a result of regression (Cooley, 1979).

The *standard errors* of parameter estimates are obtained by taking the square roots of the diagonals in the parameter covariance matrix, which is given by:

$$s^2(\mathbf{X^T W X})^{-1} \tag{2-15}$$

with $s^2$ being the error variance:

$$s^2 = \frac{\displaystyle\sum_{i=1}^{N} w_i \, (y_i^O - y_i^M)^2}{N - P} \tag{2-16}$$

where N is the number of measurements, P the number of parameters and $w_i$ the weight on observation i.

The linear correlation $r(p_1, p_2)$ between two parameters $p_1$ and $p_2$ is expressed by:

$$r(p_1, p_2) = \frac{\text{Cov}(p_1, p_2)}{\sqrt{\text{Var}(p_1)\,\text{Var}(p_2)}} \tag{2-17}$$

where the variance and covariance terms are elements of the $s^2(\mathbf{X^T W X})^{-1}$ matrix. The correlation is a measure of the inter-dependence between two parameter estimates and correlation values range between $-1$ and 1. Values close to either $-1$ or 1 mean that a change in one parameter value may be compensated for by a similar change in another parameter value to maintain the same fit (sum of squares) between model and measurements.

The standard errors and parameter correlation values are the main diagnostic measures used in this analysis when examining the parameter estimation results from evaluation of the tracer tests.

The regression analysis and statistical analysis has in this study been carried by using the program PAREST (Nordqvist, 1994). The results are presented in Chapter 4 below.

### *Handling of injection data*

All tracer injections, with the exception of the injection Rhodamine WT in CPT-4b, were made as decaying pulse injections, i.e. injection of a tracer pulse in a re-circulating system without excess pressure. Some of the injections were also accompanied by net fluid injections into the injection section. In either case, a simple and reasonable assumption is that the amount of tracer that leaves the injection section (and into the transport part) is proportional to the tracer concentration in the injection section.

The measured tracer concentrations in the injection sections were obtained by sampling at the borehole collar. Preliminary analyses indicated that these values probably are not entirely representative for the actual concentration in the injection section, most likely due to dispersion in the tubing between the injection section and the sampling. Despite this fact, it is fairly reasonable to assume that the tracer input into the transport path is at least approximately proportional to the measured injection concentrations. This assumption is employed in the analysis in this report, by defining a series of injection pulses, from the measured injection concentration curves, as described above.

The tracer injection of Rhodamine WT in CPT-4b was performed as a forced injection without circulation. For the model evaluation, the injection was defined by a single injection pulse of constant concentration.

### *Calculation of theoretical recovery*

Theoretical tracer recovery is in this study calculated as follows:

$$\text{Recovery}(\%) = 100 \text{x} \frac{Q_w}{M_{inj}} \int_0^\infty (C^{mod}(t) - C_b) dt \qquad (2\text{-}18)$$

where $Q_w$ is the flow rate from the sampling section. The tracer recovery is obtained by integrating the best-fit model breakthrough curve. The model concentration, $C^{mod}$, may be used when there is a reasonably good agreement between model and field measurements (i.e. reasonably small systematic errors in the model fit). The advantages of this are that the model breakthrough curve may be extended so that a complete recovery may be calculated, and that the model curve provides a filter for the noise in the field measurements.

### Calculation of other transport parameters

Based on the mean travel times, $t_m$, determined from the parameter estimation, the hydraulic fracture conductivity, $K_{fr}$ (m/s), were calculated assuming radial flow and validity of Darcy's law (Gustafsson & Klockars, 1981);

$$K_{fr} = \ln(r/r_w)(r^2 - r_w^2) / 2 \cdot t_m \cdot \Delta h \tag{2-19}$$

where:  $r$ = travel distance (m)

   $r_w$ = borehole radius (m)

   $t_m$ = mean travel time of tracer (s)

   $\Delta h$ = head difference (m)

The equivalent fracture aperture, $b$ (m), was calculated from:

$$b = Q \cdot t_m / \pi \cdot (r^2 - r_w^2) \tag{2-20}$$

where $Q$ (m$^3$/s), is the mean pumping rate.

Flow porosity, $\theta_k$, was calculated using:

$$\theta_k = K/K_{fr} \tag{2-21}$$

where $K$ is the hydraulic conductivity of the packed-off section of the borehole determined from steady state evaluation of the interference test (Moye, 1967):

$$K = (Q/\Delta h \cdot L) \cdot ((1 + \ln L/2r_w)/2\pi) \tag{2-22}$$

where $L$ (m) is the length of the packed-off section. It should be noted that the term flow porosity might be misleading to use in a fractured heterogeneous rock as it is defined for a porous media. However, it is often used in fractured media as a scaling factor for transport, but then defined over a finite thickness which, in his case, is defined as the length of the packed-off borehole section.

# 3 Results and interpretation

The equipment has worked well in general and no major hydraulic disturbances have occurred. Due to a major power failure in the tunnel 2003-09-23, sampling was disturbed during the pumping phase for some sections in test CPT-2. Some minor problems have also occurred related to the tracer analyses in CPT-4 where decay of tracer (Uranine) has been noted in some test tubes. The reason for this is not fully understood as handling of the samples has followed exactly the same procedure as in earlier tests at the site. Some minor problems with the sampling procedure has also occurred during the test. A Log of events during the CPT-1 to CPT-4 is presented in Table 3-1.

**Table 3-1. Log of events**

| Date | Event |
|------|-------|
| 030916 | Start tracer dilution tests **CPT-1** |
| 030917 | Start pumping KI0025F:R2, Q=3.4 l/min |
| 030919 | Stop pumping KI0025F:R2 |
| 030919 | Stop tracer dilution tests **CPT-1**, Start tracer dilution tests **CPT-2** |
| 030923 | Start pumping KI0025F02:R3, Q=1.6 l/min |
| 030925 | Stop pumping KI0025F02:R3 |
| 030925 | Stop tracer dilution tests **CPT-2**, Start tracer dilution tests **CPT-3** |
| 030930 | Start pumping KI0025F03:R3, Q=2.8 l/min |
| 031002 | Stop pumping KI0025F03:R3 |
| 031003 | Stop tracer dilution tests **CPT-3** |
|  | **Test CPT-4a** |
| 031022 | Start pumping KI0025F03:R3, Q=2.8 l/min |
| 031022 | Tracer injection in KI0025F02:R3 (Amino-G acid), KI0023B:P2 (Uranine) and KI0025F:R2 (Rhodamine Wt) |
| 031118 | Stop pumping KI0025F03:R3 |
| 031121 | Stop sampling CPT-4a |
|  | **Test CPT-4b** |
| 031118 | Start pumping KI0025F03:R3, Q=2.8 l/min |
| 031118 | Tracer injection in KA2563A:S1 (Uranine) and KA2563A:S2 (Rhodamine Wt) |
| 031120 | Tracer injection in KI0025F021:R2 (Amino-G acid) |
| 040129 | Stop sampling CPT-4b |

| Date | Event |
|------|-------|
|  | **Test CPT-4c** |
| 040128 | Tracer injection in KI0025F02:R2 (Amino-G acid) |
| 040210 | Tracer injection in KI0023B:P2 (Rhodamine Wt) |
| 040211 | Tracer injection in KI0025F02:R3 (Uranine) |
| 040227 | Stop sampling CPT-4c |



**Figure 3-1.** *Tracer injection- (left) and sampling (right) equipment.*
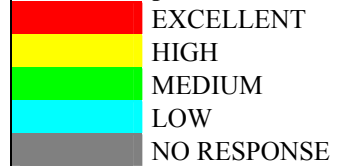
## 3.1 Pressure response matrix

The pressure response matrix for tests CPT-1 to CPT-3 is shown in Table 3-2. The matrix is based on the pressure response diagrams of each test. The colour and letter coding refers to the two indexes $s_p/Q$ (drawdown normalised to pumping rate) and $t_R/R^2$ (response time normalised to the distance squared) defined in Chapter 2.4.1.

The tests generally show high and fast responses in sections interpreted to include Structure #19, thus confirming the hydro-structural model of the TRUE Block Scale site. The main difference in response pattern is that CPT-1 gives responses in almost all sections due to the higher withdrawal and thus, larger radius of influence, of the pumping. CPT-2 and CPT-3 give very similar response patterns although some of the responses during CPT-2 are lost due to a major power failure resulting in data losses in some of the boreholes during the test. The effects of the power failure is described in more detail in Chapter 3.6.

The results of each test are discussed in more detail below. Structures #20, #21, #22 and #23 are in the text mentioned as the Structure #20-system. All the structures in the TRUE Block rock volume are presented in the hydro-structural model discussed by Andersson et al (2002a).

**Table 3-2. Pressure response matrix for CPT-1 through CPT-3.**

| Sink in Structure | | # 19 | # 19 | # 19 | |
|---|---|---|---|---|---|
| Borehole | Interval (m) | CPT-1 | CPT-2 | CPT-3 | Structure |
| KA2511A:T1 | 239-293 | B | | | # 10,11,18 |
| KA2511A:T2 | 171-238 | B | | | # 19 |
| KA2511A:T3 | 139-170 | B | | | # ? |
| KA2511A:T4 | 111-138 | B | | | # 20 |
| KA2511A:T5 | 103-110 | B | | | # 16 |
| KA2511A:T6 | 96-102 | B | | | # 6 |
| KA2511A:T7 | 65-95 | B | | | # ? |
| KA2511A:T8 | 6-64 | B | | | # 4, 7 |
| KA2563A:S1 | 242-246 | G | G | G | # 19 |
| KA2563A:S2 | 236-241 | G | G | G | # 19 |
| KA2563A:S3 | 206-208 | B | B | B | # 13 |
| KA2563A:S4 | 187-190 | B | | B | # 20 |
| KA2563A:S5 | 146-186 | B | | | # 6, 7 |
| KI0025F:R1 | 170.5-193.66 | B | M | M | Z |
| KI0025F:R2 | 165.5-169.5 | S | G | G | # 19 |
| KI0025F:R3 | 90.5-164.5 | E | B | M | ? |
| KI0025F:R4 | 87.5-89.5 | B | B | B | # 20, 22 |
| KI0025F:R5 | 42.5-86.5 | B | | | # 6, 7 |
| KI0025F:R6 | 5-41.5 | B | | | # 5 |
| KI0023B:P1 | 113.7-200.7 | B | | | # 10 |
| KI0023B:P2 | 111.25-112.7 | G | E | E | # 19 |
| KI0023B:P3 | 87.20-110.25 | B | G | G | ? |
| KI0023B:P4 | 84.75-86.20 | B | B | B | # 13 |
| KI0023B:P5 | 72.95-83.75 | B | B | B | # 18 |
| KI0023B:P6 | 70.95-71.95 | B | B | B | # 21 |
| KI0023B:P7 | 43.45-69.95 | B | B | B | # 6, 20 |
| KI0023B:P8 | 41.45-42.45 | B | | | # 7 |
| KI0023B:P9 | 4.6-40.45 | B | | | # 5 |
| KI0025F02:R1 | 140.05-204.18 | B | | B | # ? |
| KI0025F02:R2 | 135.1-139.05 | B | B | B | # 25 |
| KI0025F02:R3 | 129.2-134.1 | G | S | E | # 19 |
| KI0025F02:R4 | 100.25-128.2 | T i g h t | | | |
| KI0025F02:R5 | 93.35-99.25 | B | B | B | # 13, 21 |
| KI0025F02:R6 | 78.25-92.35 | T i g h t | | | |
| KI0025F02:R7 | 73.3-77.25 | B | | B | # 20 |
| KI0025F02:R8 | 64.0-72.3 | B | B | B | # 22 |
| KI0025F02:R9 | 56.1-63.0 | | | B | # 23 |
| KI0025F02:R10 | 3.4-55.1 | B | | | # 5, 6, 7 |
| KI0025F03:R1 | 135.03-141.72 | B | M | G | # ? |
| KI0025F03:R2 | 129.03-134.03 | B | | B | # 25 |
| KI0025F03:R3 | 123.03-128.03 | G | G | S | # 19 |
| KI0025F03:R4 | 93.53-122.03 | B | | B | # ? |
| KI0025F03:R5 | 89.03-92.53 | B | B | B | # 13 |
| KI0025F03:R6 | 75.03-88.03 | B | | B | # 21 |
| KI0025F03:R7 | 66.53-74.03 | B | | B | # 20 |
| KI0025F03:R8 | 59.53-65.53 | B | B | B | # 22 |
| KI0025F03:R9 | 55.03-58.53 | | | | # 23 |
| KA3510A:R1 | 125-150.06 | | | | # ? |
| KA3510A:R2 | 110-124 | B | | | # 15 |
| KA3510A:R3 | 75-109 | B | | | # ? |
| KA3510A:R4 | 51-74 | B | | | # 6, 8 |
| KA3510A:R5 | 4.5-50 | B | | | # 3, 4, 5 |

**INDEX 1=sp/Q**

| | |
|---|---|
| (red) | EXCELLENT |
| (yellow) | HIGH |
| (green) | MEDIUM |
| (cyan) | LOW |
| (gray) | NO RESPONSE |

**INDEX 2=tr/R2**

E=EXCELLENT
G=GOOD
M=MEDIUM
B=BAD

S=SINK

## 3.2 Test CPT-1

The first test, CPT-1, was performed by pumping borehole section KI0025F:R2 (Structure #19), located farthest to the east of the boreholes in the TRUE Block Scale array. Pressure responses (>1 kPa) were registered in almost all of the 49 borehole sections within, cf. Figure 2-2. the TRUE Block Scale array over distances ranging between 15 to 230 m.

The response pattern (Figure 3-2) generally confirms the hydro-structural model with high and fast responses in sections interpreted to include Structure #19. The magnitude of the hydraulic responses in Structure #19 is typically between 4-25 kPa and in Structure 25, 10-37 kPa. Responses in other section/structures (Structure #20-system) are less than 7 kPa. However, there are some responses that do not follow this pattern, in particular the very good responses in KI0025F:R3 (64 kPa), KI0025F:R1 (42 kPa) and KI0025F03:R1 (34 kPa) indicating that these may be splay fractures to Structure #19.
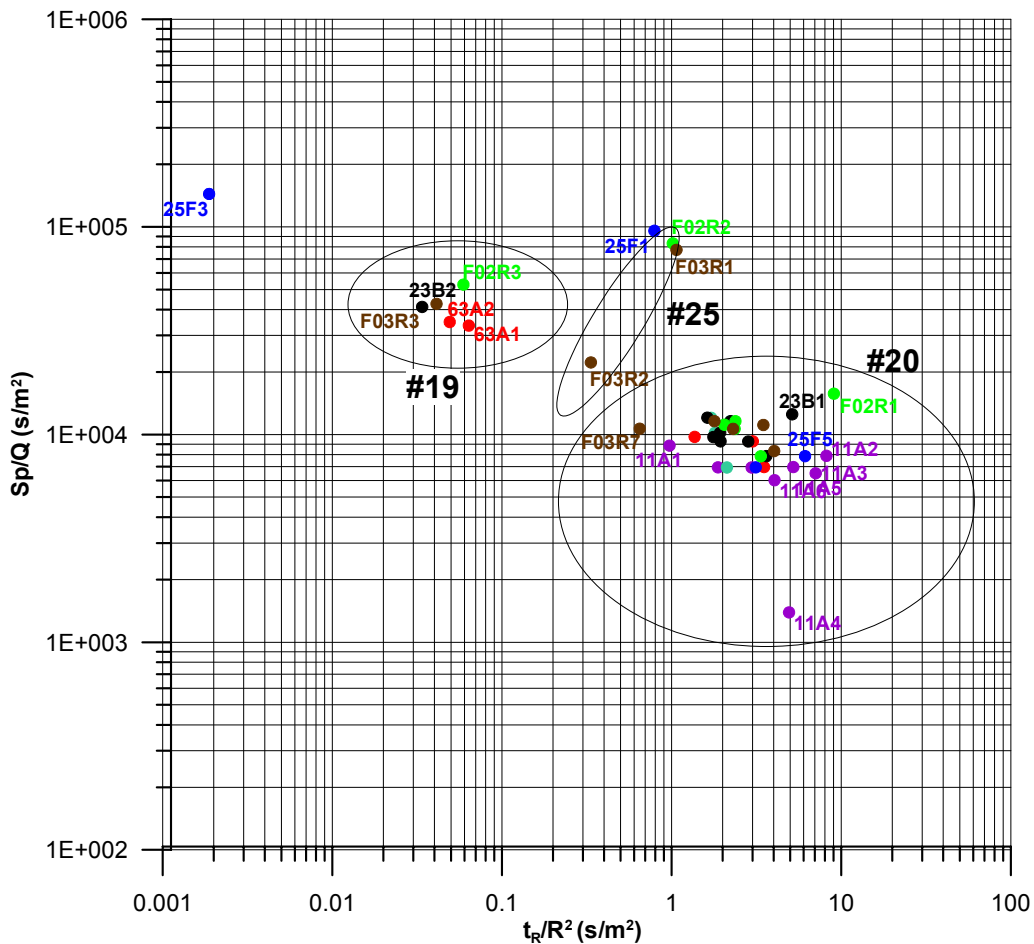


*Figure 3-2. Diagnostic plot of pressure responses during test CPT-1. The encircled areas mark the responses of some of the structures. Borehole notations are shortened by removing the prefix "KI0025-", KI0023- and "KA25-" from the borehole labels, cf. Table 3-2.*

The pump rate and the electrical conductivity as a function of time are shown in Figure 3-3. The pumping flow rate was almost constant, 3.4 l/min, during the pumping period. An increase in the electrical conductivity from 1340 to 1420 mS/m indicates an increasing influx of saline water.
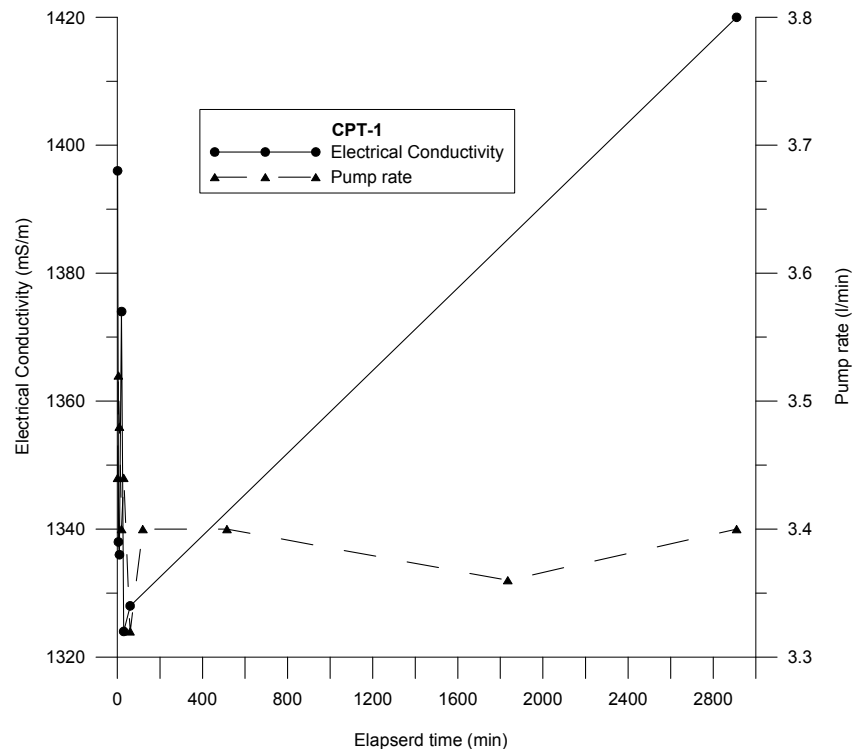


*Figure 3-3. Pump rate and electrical conductivity of the pumped water from KI0025F:R2 during test CPT-1.*

Test CPT-1 also included measurements of flow rates using the tracer dilution method in seven selected observation sections. In Figure 3-4 the sinks and sources for CPT-1 – CPT-3 are shown together with the boreholes and the main structures. The measurements were performed both under natural gradient conditions and during pumping of section KI0025F:R2 (Structure #19) in order to study the influence of the pumping. The results presented in Table 3-3 show a distinct influence in some of the tested sections especially in KI0025F03:R3 (Structure #19) and in KI0025F03:R2 (Structure #25), see also Figure 3-5. The latter section has a negative flow response indicating a change in flow direction. The other sections show minor changes in flow rate.
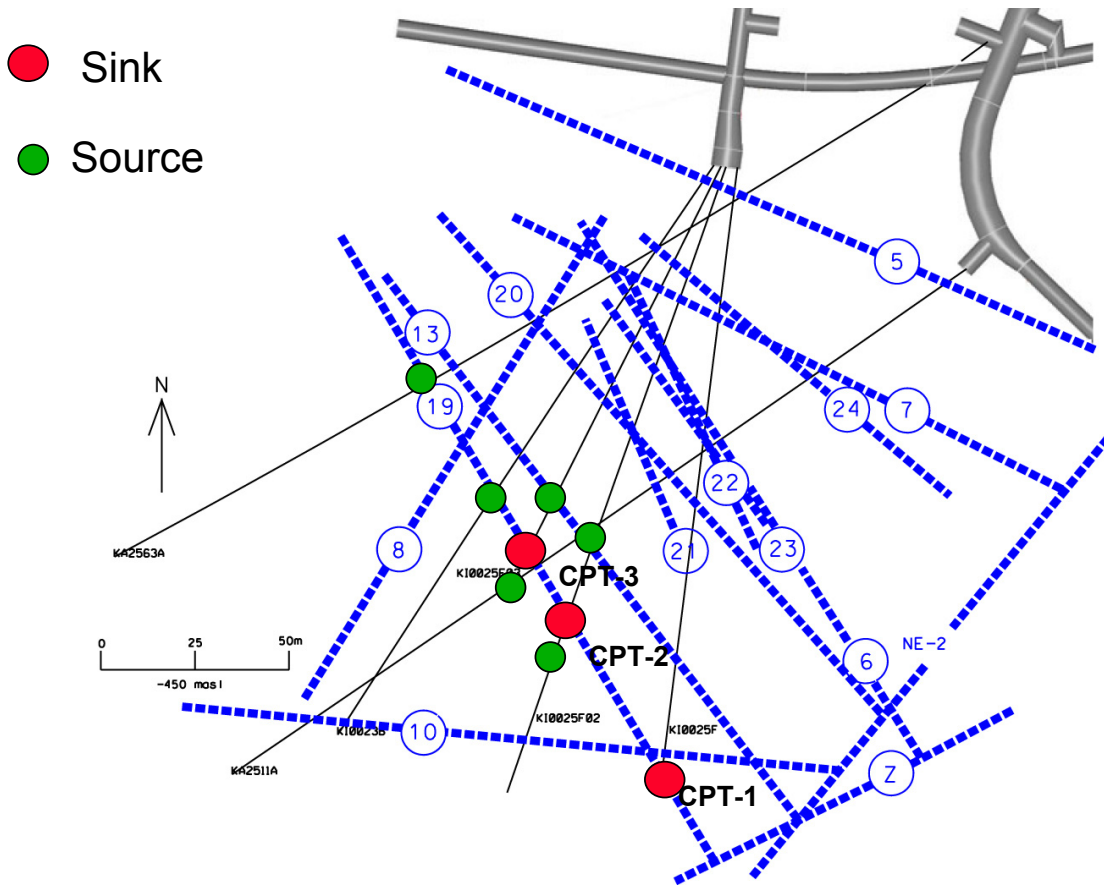
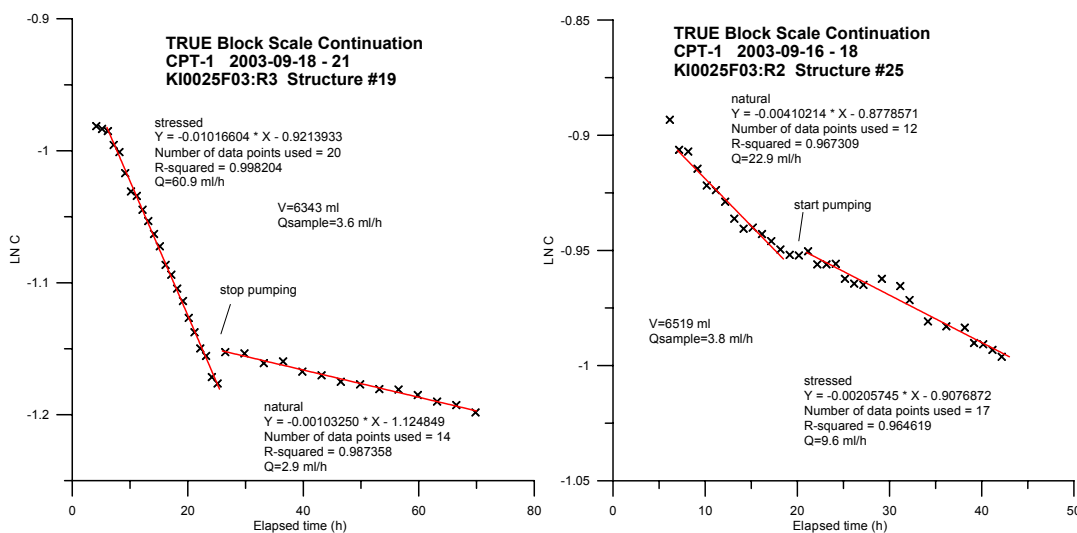**Figure 3-4.** *Sinks and sources in True Block Scale pre-tests CPT-1 through CPT-3.*



**Figure 3-5.** *Examples of tracer dilution graphs (Logarithm of concentration versus time) for sections KI0025F03:R3 (Structure #19) and KI0025F03:R2 (Structure #25). Steeper dip of the straight-line fit implies a higher flow rate.*

**Table 3-3. Results of tracer dilution tests during CPT-1, using KI0025F:R2 (Structure #19) as sink.**

| Test section | Structure # | Section volume (ml) | $Q_{natural}$ (ml/h) | $Q_{stressed}$ (ml/h) | $\Delta Q$ (ml/h) |
|---|---|---|---|---|---|
| KA2563A:S1 | 19 | 8814 | 17 | 12 | - 5 |
| KI0023B:P2 | 19 | 3621 | 26 | 30 | + 4 |
| KI0025F:R2 | 19 | 7210 | | SINK | |
| KI0025F02:R2 | 25 | 7141 | 40 | 44 | + 4 |
| KI0025F02:R3 | 19 | 7747 | 11 | 9 | - 2 |
| KI0025F02:R5 | 13,21 | 7856 | 9 | 8 | - 1 |
| KI0025F03:R2 | 25 | 6519 | 23 | 10 | - 13 |
| **KI0025F03:R3** | **19** | **6343** | **3** | **61** | **+ 58** |

## 3.3 Test CPT-2

Test CPT-2, performed by pumping borehole section KI0025F02:R3 (Structure #19), shows pressure responses (>1 kPa) in 20 borehole sections within the TRUE Block Scale site over distances ranging between 5 and 67 m.

The response pattern during this test generally confirms the hydro-structural model in a similar way as in CPT-1 although the radius of influence of the pumping is smaller compared to test CPT-1. All of the sections responding fast and good (in the upper left corner of Figure 3-6) are interpreted as being associated with Structure #19. Structure #25 responds high but slow and notably, only in one of the sections interpreted as being connected to the structure. This suggests that this is not one structure but rather two separate single fractures having a similar orientation and both being connected individually to Structure #19.

The magnitudes of the hydraulic responses in Structures #19 are typically between 2-55 kPa whereas responses in Structure #20-system are less than 5 kPa. However, there are some responses that do not follow this pattern, in particular the noted good responses in KI0023B:P3 (18 kPa), KI0025F:R3 (8 kPa) and KI0025F03:R1 (13 kPa) indicating that these may be splay fractures to Structure #19 or other structures connected to #19. In the current hydro-structural model the conductive structures in all three sections are noted as unknown, meaning that the intercept cannot be connected to a structure in another borehole.

The pumping flow rate decreased from 1.9 l/min to about 1.6 l/min during the pumping period. The electrical conductivity was almost constant, 1375 mS/m, cf. Figure 3-7.
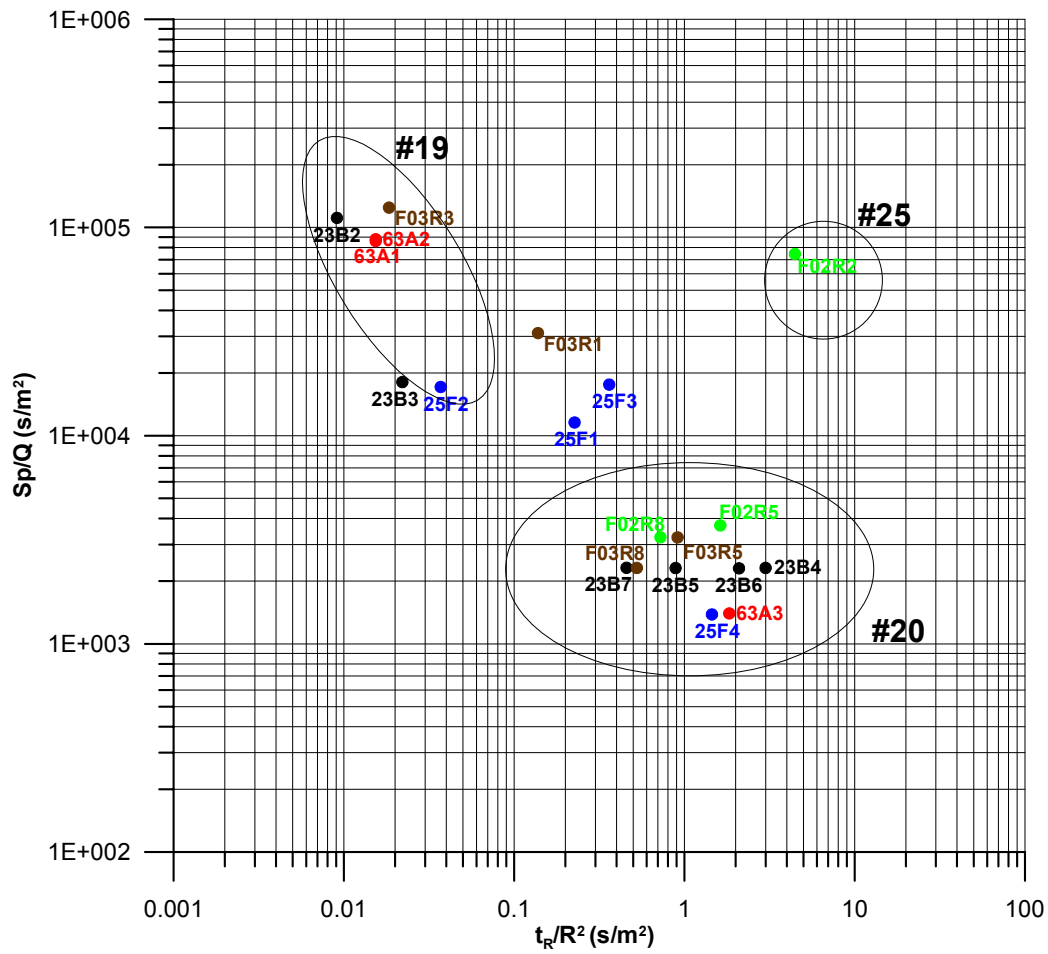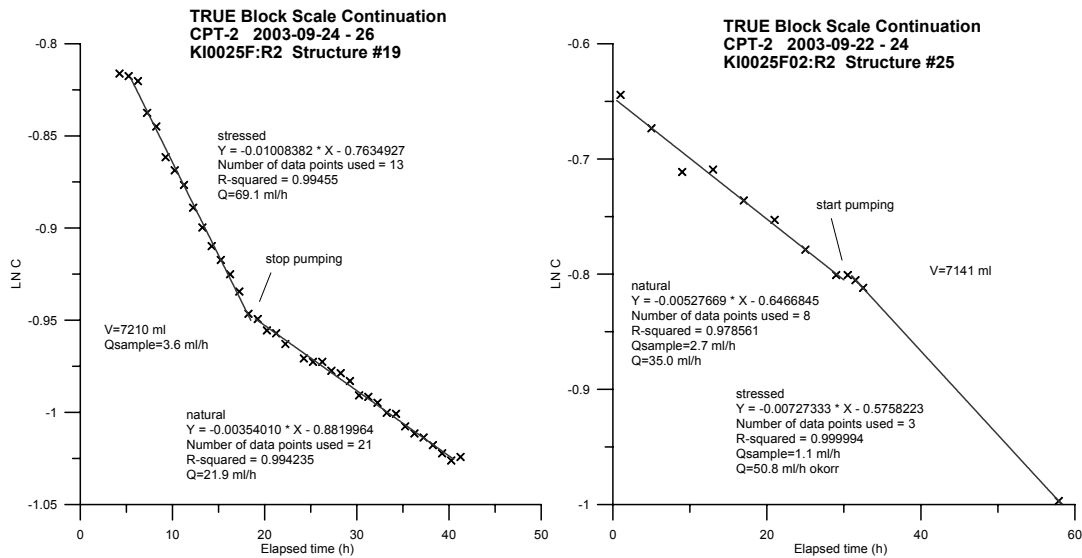
***Figure 3-6.*** *Diagnostic plot of pressure responses during test CPT-2. The encircled areas mark the responses of different structures, or groups of structures. Borehole notations are shortened by removing the prefix "KI0025-", KI0023- and"KA25-" from the borehole labels, cf. Table 3-2.*
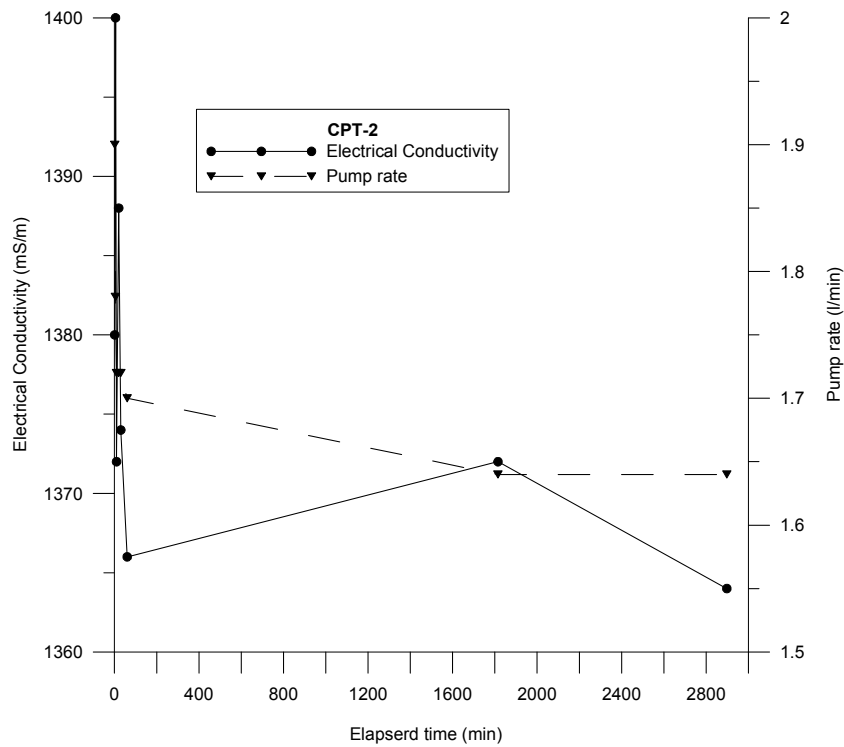
*Figure 3-7. Pump rate and electrical conductivity of the pumped water from KI0025F02:R3 during test CPT-2.*

Test CPT-2 included measurements of flow rates using the tracer dilution method in eight selected observation sections. The measurements were performed both under natural gradient and during pumping of section KI0025F02:R3 (Structure #19) in order to study the influence of the pumping. The test was disturbed by the long power failure and resulting loss of samples during the pumping phase in four of the sections. The results presented in Table 3-4 show a distinct increase in flow in most of the tested sections, except in sections associated with Structures #13 and #21 (KI0025F02:R5 and KI0025F03:R5) and also in KI0025F03:R2 associated with structure #25. The latter lack of response is also consistent with the lack of pressure response discussed earlier in this section. Examples of tracer dilution curves are shown in Figure 3-8.

**TRUE Block Scale Continuation**
CPT-2  2003-09-24 - 26
KI0025F:R2  Structure #19

stressed
Y = -0.01008382 * X - 0.7634927
Number of data points used = 13
R-squared = 0.99455
Q=69.1 ml/h

stop pumping

V=7210 ml
Qsample=3.6 ml/h

natural
Y = -0.00354010 * X - 0.8819964
Number of data points used = 21
R-squared = 0.994235
Q=21.9 ml/h

**TRUE Block Scale Continuation**
CPT-2  2003-09-22 - 24
KI0025F02:R2  Structure #25

start pumping

V=7141 ml

natural
Y = -0.00527669 * X - 0.6466845
Number of data points used = 8
R-squared = 0.978561
Qsample=2.7 ml/h
Q=35.0 ml/h

stressed
Y = -0.00727333 * X - 0.5758223
Number of data points used = 3
R-squared = 0.999994
Qsample=1.1 ml/h
Q=50.8 ml/h okorr

*Figure 3-8. Examples of tracer dilution graphs (Logarithm of concentration versus time) for sections KI0025F:R2 (Structure #19) and KI0025F02:25 (Structure #25). Steeper dip of the straight-line fit implies a higher flow rate.*

**Table 3-4. Results of tracer dilution tests during CPT-2, using KI0025F02:R3 (Structure #19) as sink. Figures in italics are somewhat uncertain due to disturbed sampling caused by a power failure.**

| Test section | Structure # | Section volume (ml) | $Q_{natural}$ (ml/h) | $Q_{stressed}$ (ml/h) | $\Delta Q$ (ml/h) |
|---|---|---|---|---|---|
| KA2563A:S1 | 19 | 8814 | 5 | 14 | + 9 |
| KI0023B:P2 | 19 | 3621 | 23 | *33* | + 10 |
| KI0025F:R2 | 19 | 7210 | 22 | 69 | + 47 |
| KI0025F02:R2 | 25 | 7141 | 35 | *51* | + 16 |
| KI0025F02:R3 | 19 | 7747 | | **SINK** | |
| KI0025F02:R5 | 13,21 | 7856 | 18 | 18 | ± 0 |
| KI0025F03:R2 | 25 | 6519 | 7 | 8 | + 1 |
| KI0025F03:R3 | 19 | 6343 | 3 | *423* | + 420 |
| **KI0025F03:R5** | **13** | **4912** | **9** | *2* | **- 7** |

## 3.4    Test CPT-3

Test CPT-3, performed by pumping borehole section KI0025F03:R3 (Structure #19), shows pressure responses (>1 kPa) in a total of 28 borehole sections within and outside the TRUE Block Scale Site over distances ranging between 5 and 70 m.

The responses presented in Figure 3-9 are clearly separated in three classes. The first, showing high, and in most cases fast, responses, belong to sections associated with Structure #19 and, as in CPT-2, also sections KI0023B:P3, KI0025F:R1 and KI0025F:R3. The second class includes all the remaining sections in the TRUE Block Scale array including the Structure #20-system and the third class shown in Figure 3-9 are the high but slow responding sections in Structure #25. Notable is that both sections connected to #25 responds in contrast to CPT-2 where only one of the sections responded. The magnitudes of the hydraulic responses in Structures #19 are typically between 12-100 kPa whereas responses in Structure #20-system are less than 3 kPa.

The flow rate decreased from 3.00 to 2.84 l/min during the pumping period of CPT-3, cf. Figure 3-10. The electrical conductivity ranged between 1360 and 1390 mS/m and is almost constant during the test.
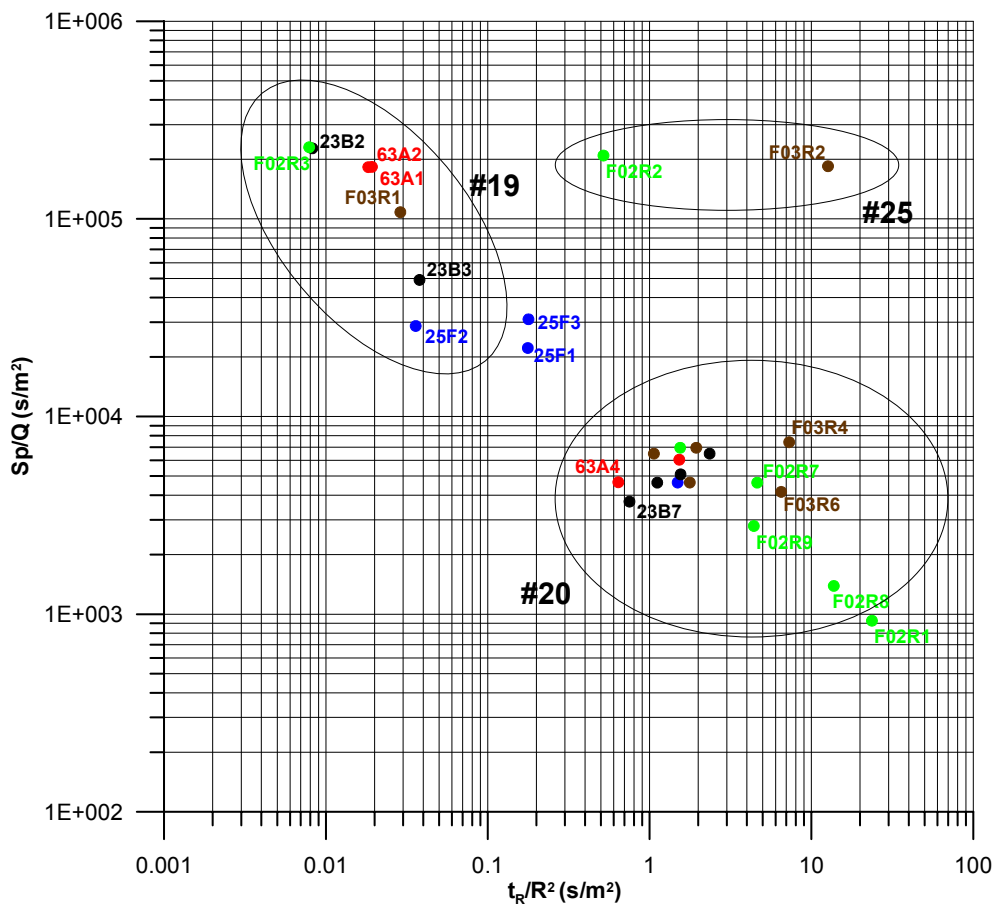


**Figure 3-9.** *Diagnostic plot of pressure responses during test CPT-3. The encircled areas mark the responses of different structures. Borehole notations are shortened by removing the prefix "KI0025-", "KI0023- and"KA25-" from the borehole labels, cf. Table 3-2.*

41
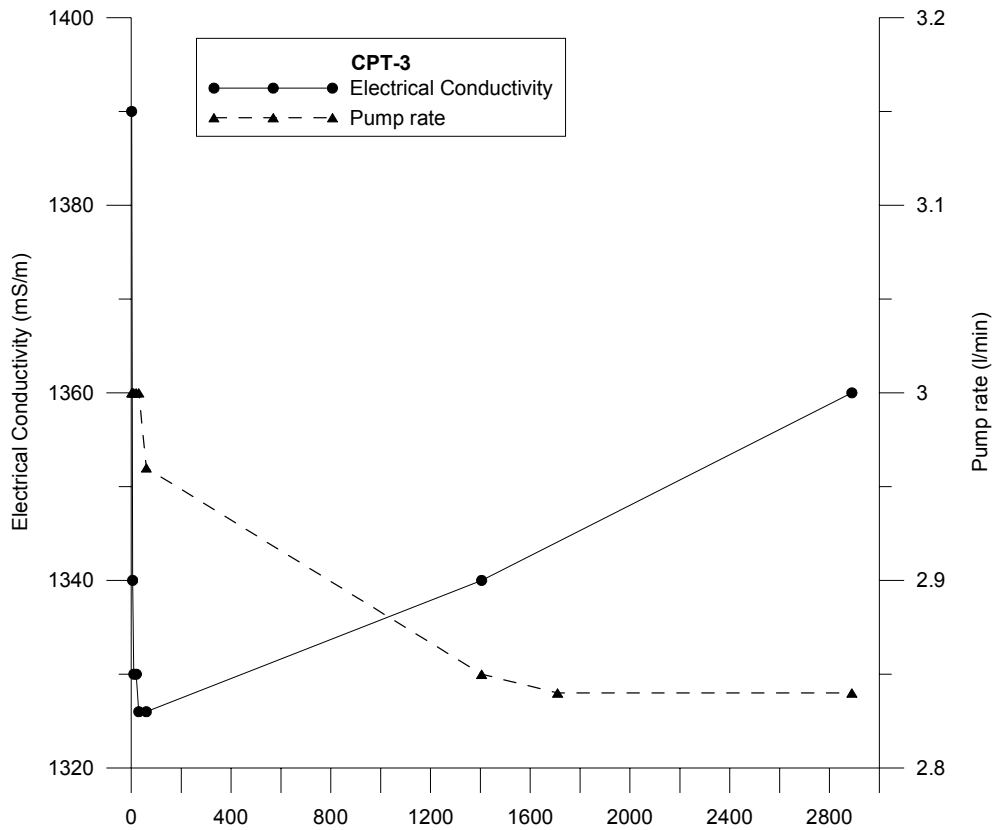
**Figure 3-10.** *Pump rate and electrical conductivity of the pumped water from KI0025F03:R3 during test CPT-3.*

Test CPT-3 included measurements of flow rates using the tracer dilution method in eight selected observation sections. The measurements were performed both under natural gradient and during pumping of section KI0025F03:R3 (Structure #19) in order to study the influence of the pumping, see examples in Figure 3-11. The results presented in Table 3-5 show a distinct increase in all of the tested sections except in KI0025F02:R5 (Structure #13 and #21) where the flow is decreased and in KI0025F02:R2 (Structure #25) where the flow is constant. The latter flow rate is surprisingly high considering the low transmissivity of the structure. Expected flow rates should be around 10 times lower as in KI0025F03:R2. One possible explanation for this is that the pressure in the borehole interval is lowered as a consequence of a partly clogged filter located at the inlet of the circulation loop close to the upper packer. This lowering of the pressure can be seen in the pressure plots and amounts to about 25 kPa, thus creating a forced gradient around the borehole with increased flow rates.
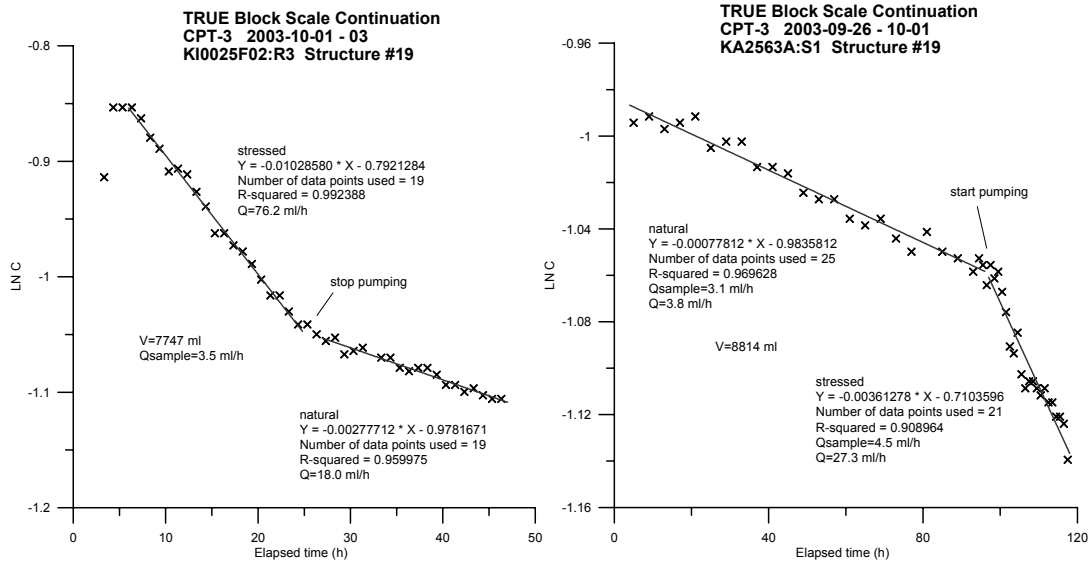
**Figure 3-11.** *Examples of tracer dilution graphs (Logarithm of concentration versus time) for sections KI0025F02:R3 (Structure #19) and KA2563A:S1 (Structure #19), test CPT-3. Steeper dip of the straight-line fit implies a higher flow rate.*

**Table 3-5. Results of tracer dilution tests during CPT-3, using KI0025F03:R3 (Structure #19) as sink.**

| Test section | Structure # | Section volume (ml) | $Q_{natural}$ (ml/h) | $Q_{stressed}$ (ml/h) | $\Delta Q$ (ml/h) |
|---|---|---|---|---|---|
| KA2563A:S1 | 19 | 8814 | 4 | 27 | **+ 23** |
| KI0023B:P2 | 19 | 3621 | 18 | 31 | **+ 13** |
| KI0025F:R2 | 19 | 7210 | 22 | 85 | **+ 63** |
| KI0025F02:R2 | 25 | 7141 | 42 | 42 | **± 0** |
| KI0025F02:R3 | 19 | 7747 | 18 | 76 | **+ 58** |
| KI0025F02:R5 | 13,21 | 7856 | 30 | 18 | **- 12** |
| KI0025F03:R2 | 25 | 6519 | 6 | 9 | **+ 3** |
| KI0025F03:R3 | 19 | 6343 | **SINK** | | |
| **KI0025F03:R5** | **13** | **4912** | **4** | **6** | **+ 2** |

43

## 3.5    Test CPT-4

Test CPT-4 was divided into three separate batches of tracer injections including three injections in each batch (CPT-4a-c). The last batch of injections, CPT-4c, included re-runs in three of the earlier tested flow paths but with partly changed flow geometry. The tests were performed as cross-hole tracer tests using KI0025F03:R3 (Structure #19) as sink, cf. Figure 3-12. The selection of sink was based on the results of CPT-1 through CPT-3 where the selected section gave the best hydraulic and flow responses and also the best possibilities to use different geometries.

The tests were performed in a radially converging flow field with a withdrawal rate of Q=2.8 l/min at the start of CPT-4a in September 2004 and slowly decreasing to Q=2.6 l/min until the stop of CPT-4c in March 2004. Some of the injections were also accompanied by net fluid injections into the injection section in order to avoid excessive tailing of the injection function.
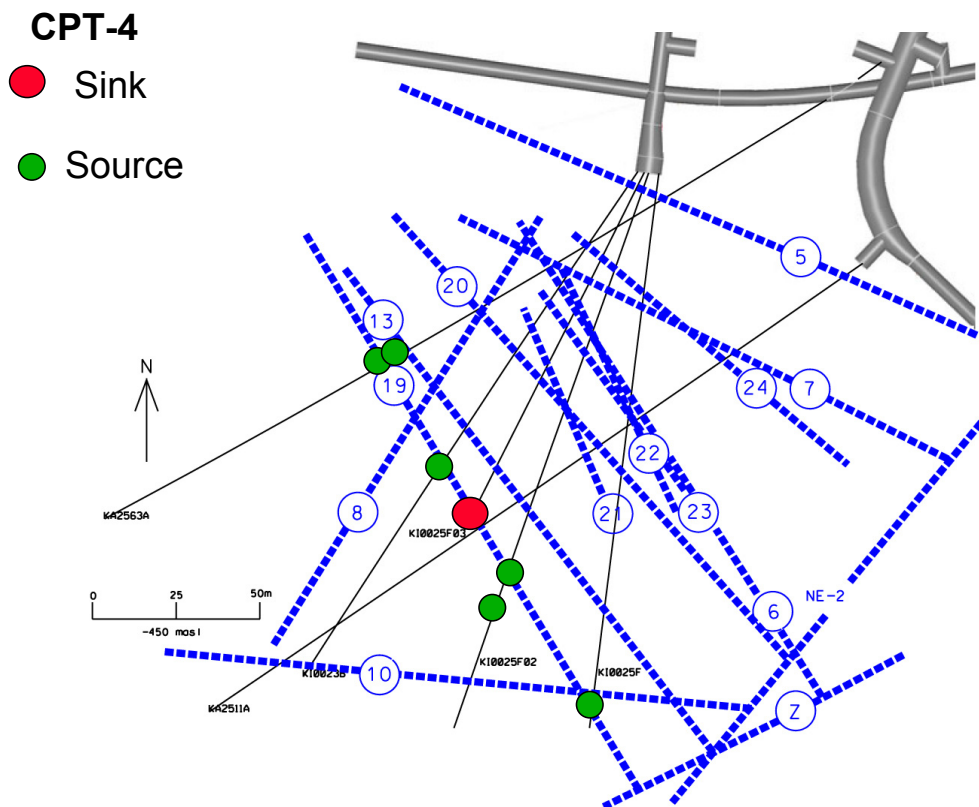


*Figure 3-12. Horizontal section at Z=–450 masl (meters above sea level) showing the structural model based on identified conductive geological structures in the TRUE Block Scale rock volume and location of pumping (sink) and injection (source) sections in pre-test CPT-4.*
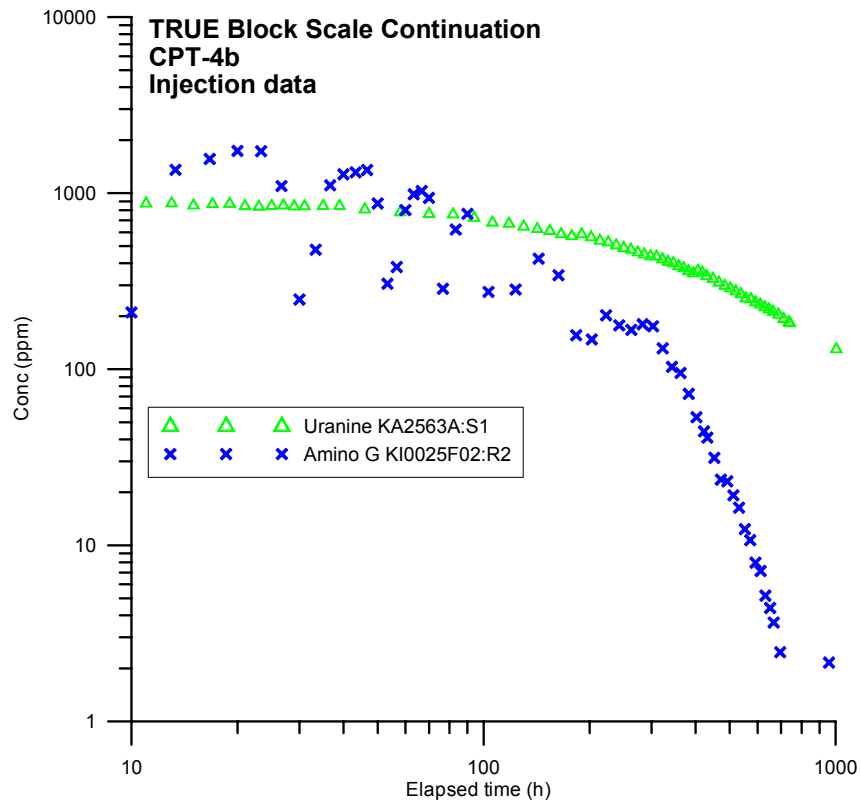
### 3.5.1    Tracer injections

The nine tracer injections were performed without major disturbances with the exception of one where a pump failure occurred, cf. below. The three injections during CPT-4a were all performed without excess pressure (decaying pulse). The tracer solutions in the injection intervals were exchanged with unlabelled water after about
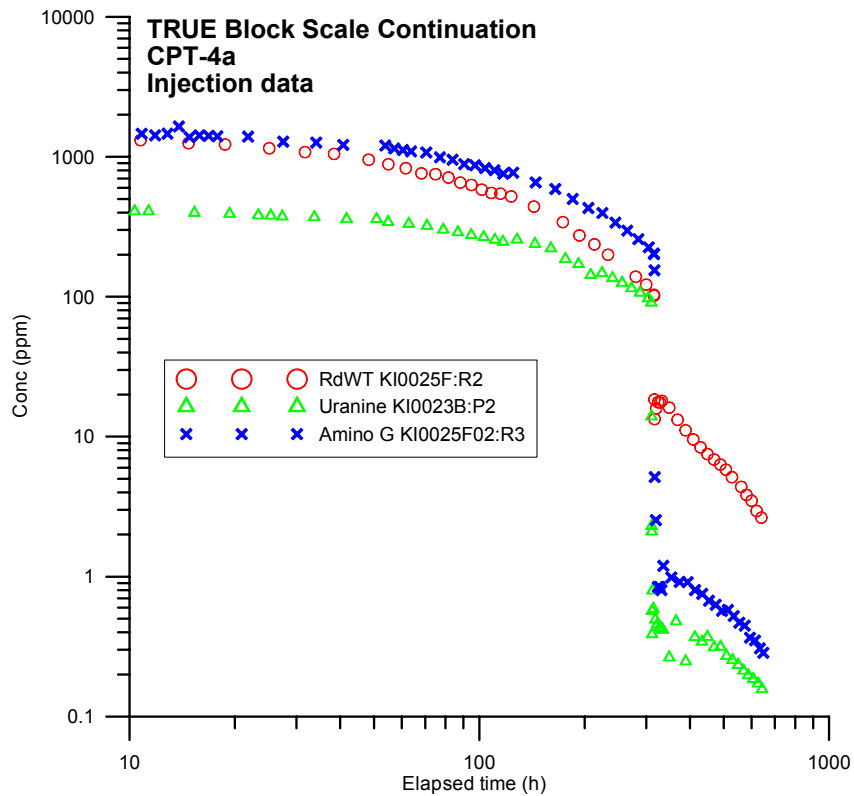
*Figure 3-13.* *CPT-4a-tracer injection curves for injections (log-log scale).*

In test CPT-4b the injection in KA2563A:S1 was performed as a decaying pulse whereas the injection in KA2563A:S2 was performed by injecting a pulse of concentrated tracer solution and flushing/injecting the solution into the borehole by means of 25 litres of unlabelled water. This procedure was applied as only one flow line was available and thus no circulation of tracer was possible. Consequently, no samples could be taken on the input concentration in the section. The third tracer injection, performed in Structure #25, was made as a decaying pulse accompanied by a constant injection of water (2 ml/min) into the injection interval KI0025F02:R2. A pump failure occurred in the test during injection in KI0025F02:R2 between 193 h and 288 h after start of injection, causing an almost complete stop in the mass flux from the injection section. This fact together with the initial high and varying background signal in the fluorescence measurement of the tracer Amino G Acid induced some uncertainties in the measured recovery. For these reasons, it was decided to repeat this injection in test CPT-4c.

The graph of the tracer injection concentrations versus time for CPT-4b (Figure 3-14) also reveal that the mixing in section KI0025F02:R2 is somewhat poor due to problems with a clogged filter as earlier mentioned in connection to tracer dilution test CPT-3.
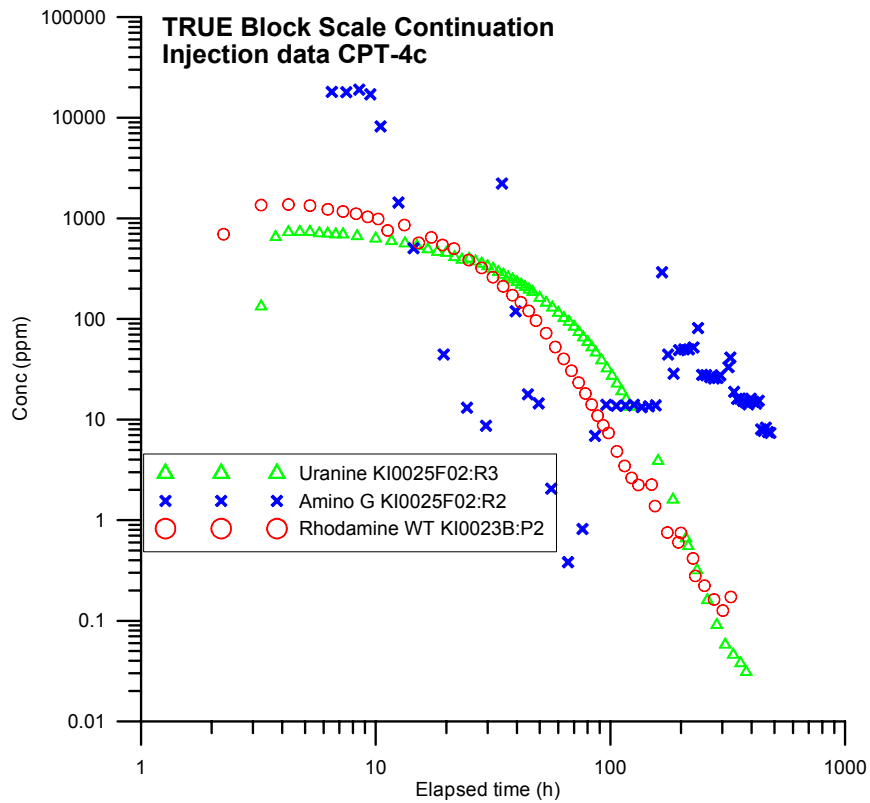
**Figure 3-14.** *CPT-4b-tracer injection curves for injections (log-log scale).*

Test CPT-4c was performed as a decaying pulse, like in CPT-4a, though this time with an accompanying injection of water in all three selected injection sections. The main reason for adding extra water to the injection was to shorten the tracer residence time in the injection section. This is a necessary prerequisite for the performance of later injections with radioactive sorbing tracers and the repeated injections were done to verify that tracer mass recovery was >80%. This mass recovery is necessary to achieve for radiation safety aspects of the forthcoming tracer tests with radioactive sorbing tracers.

The injection concentrations of CPT-4c presented in Figure 3-15 and Table 3-6 are the actually measured ones and based on those, a flow rate was calculated from the dilution of tracer versus time (Table 3-5). Notable is again that the injection concentration in KI0025F02:R2 varies significantly at earlier times due to the relatively poor mixing in the section. This is also reflected by the flow rate calculated from the dilution of tracer versus time where the injection of water was set to (and calibrated to) 2 ml/min while the calculated (mass flux) is only about 0.4 ml/min. For the other two injection sections the calculated flow rates compare better with the actually added (about 4 ml/min compared to 5 ml/min added). This difference has earlier been observed in previous experiments using this set-up and may also be explained by poor mixing so that a portion of the unlabelled water added is injected without complete mixing with the rest of the volume in the injection section.

46

***Figure 3-15.*** *CPT-4c-tracer injection curves for injections (log-log scale).*

**Table 3-6. Tracer injection data for test CPT-4a - CPT-4c (measured values).**

| Test | Inj. Section | Struct. | Tracer | Max inj. conc. (mg/l) | Inj. rate (ml/h) | Inj. mass (mg) | Section volume (ml) |
|------|--------------|---------|--------|-----------------------|------------------|----------------|---------------------|
| CPT-4a | KI0025F:R2 | #19 | Rhodamine WT | 1367 | 50 | 12650 | 7210 |
| | KI0025F02:R3 | #19 | Amino-G Acid | 1647 | 33 | 12400 | 7747 |
| | KI0023B:P2 | #19 | Uranine | 414 | 15 | 1300 | 3621 |
| CPT-4b | KA2563A:S1 | #19 | Uranine | 888 | 19 | 7830 | 8814 |
| | KA2563A:S2 | #19 | Rhodamine WT | 20000 | 600 | 10900 | 12588 |
| | KI0025F02:R2 | #25 | Amino-G Acid | 1739 | 72 | 15400 | 7141 |
| CPT-4c | KI0025F02:R3 | #19 | Uranine | 733 | 262 | 7290 | 7747 |
| | KI0023B:P2 | #19 | Rhodamine WT | 1370 | 213 | 6300 | 3621 |
| | KI0025F02:R2 | #25 | Amino-G Acid | 18000 | 25 | 17300 | 7141 |

47

### 3.5.2 Tracer breakthrough

Breakthrough has been monitored in KI0025F03:R3 from all three injection points in test CPT-4a. The breakthrough data for Amino G and Rhodamine WT have been quality assured whereas the data for Uranine are uncertain. The reason for this is that Uranine has been subject to some degradation in the test tubes and also possibly due to contamination of the sampling equipment which have caused disturbances in the breakthrough data due to. The latter effect showed up in the tail of the breakthrough curve when sampling times were decreased from 4 hours to 30 minutes. This contamination results in a mass recovery of more than 100% (cf. Table 3-7). Breakthrough curves from the three injections in CPT-4a are shown in Figures 3-16 and 3-17. The lack of data in the graphs is due to problems with the automatic sampler.
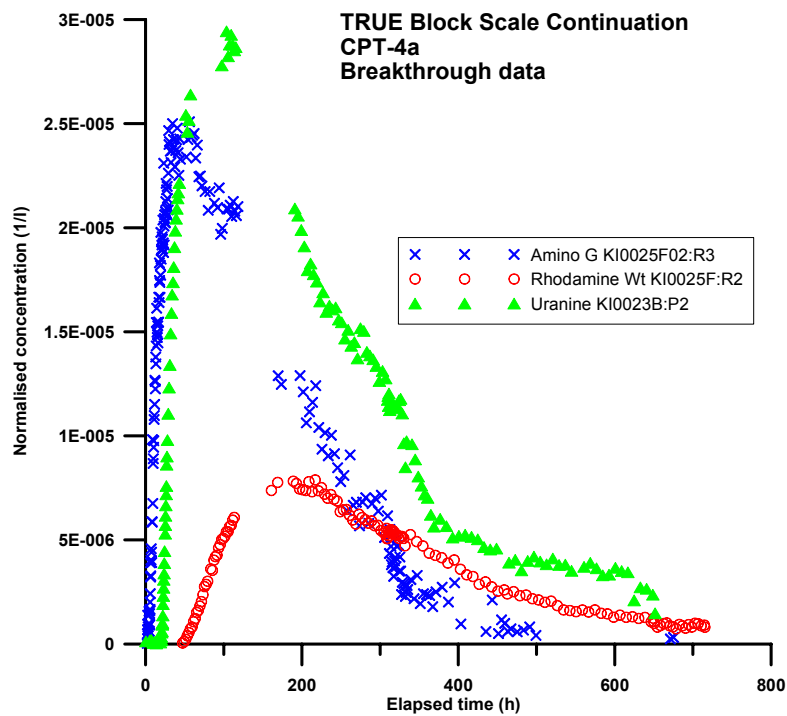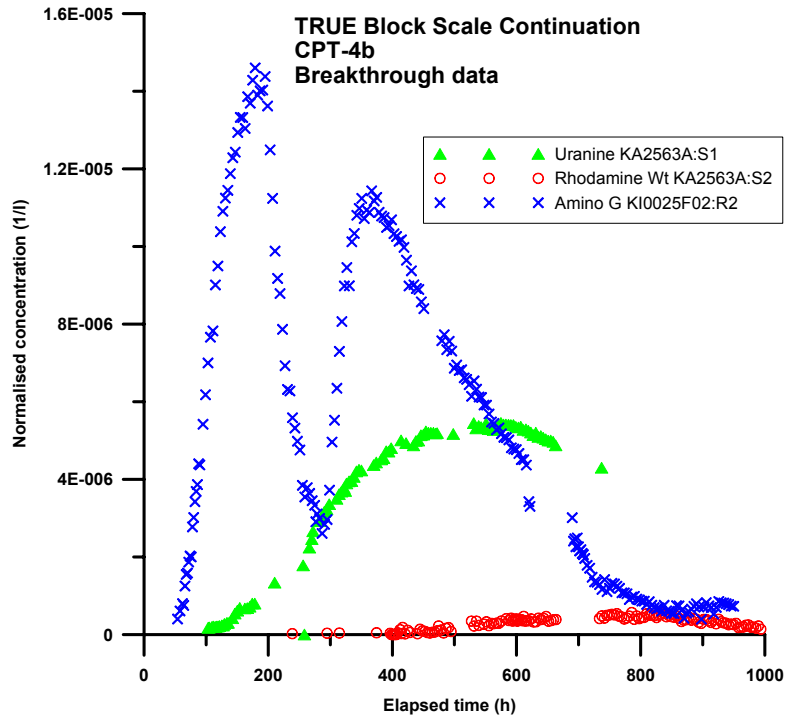


***Figure 3-16.*** *Tracer breakthrough curves for test CPT-4a, injection in KI0025F02:R3 (blue), KI0023B:P2 (green) and KI0025F:R2 (red), linear time scale. Concentrations are normalised to injected mass.*
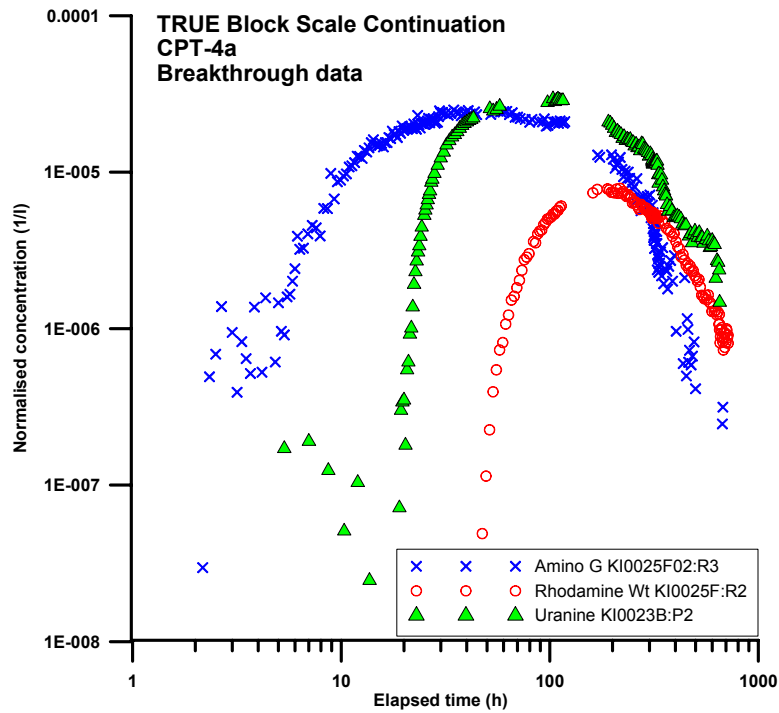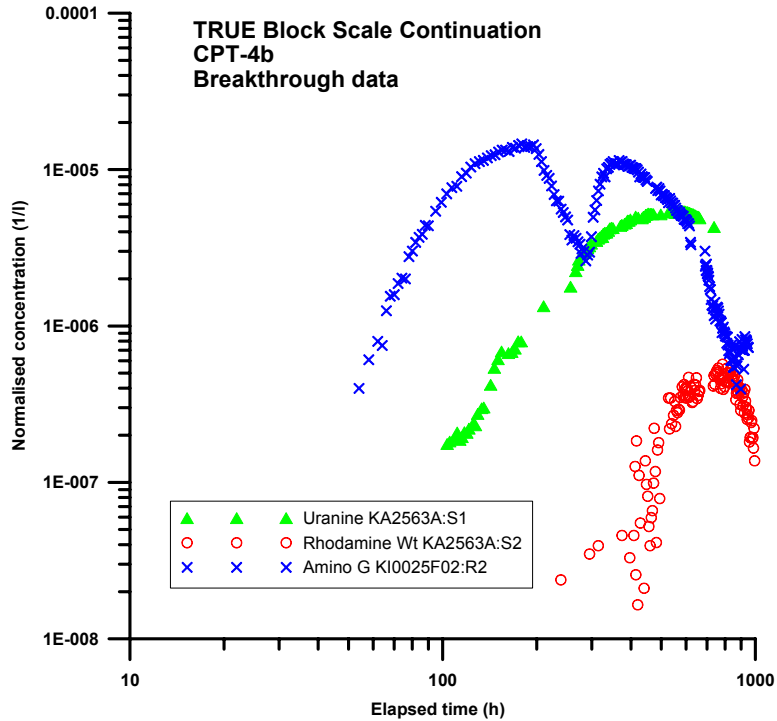
*Figure 3-17.* *Tracer breakthrough curves for test CPT-4a, injection in KI0025F02:R3 (blue), KI0023B:P2 (green) and KI0025F:R2 (red), logarithmic time scale. Concentrations are normalised to injected mass.*

Breakthrough has also been monitored from all three injection points in CPT-4b. Also here the Uranine data should be regarded as uncertain due to degradation in the test tubes. Breakthrough curves from the three injections in CPT-4b are shown in Figures 3-18 and 3-19. The dip of Amino-G data after the peak in the graphs is due to a pump failure during injection in KI0025F02:R2.
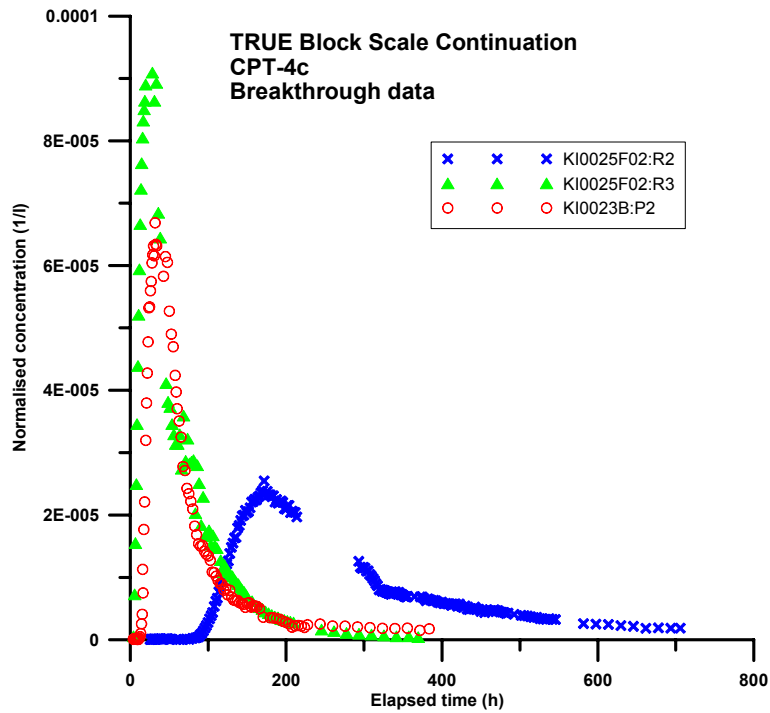
***Figure 3-18.*** *Tracer breakthrough curves for test CPT-4b, injection in KI0025F02:R2 (blue), KA2563A:S1 (green) and KA2563A:S2 (red), linear time scale. Concentrations are normalised to injected mass.*
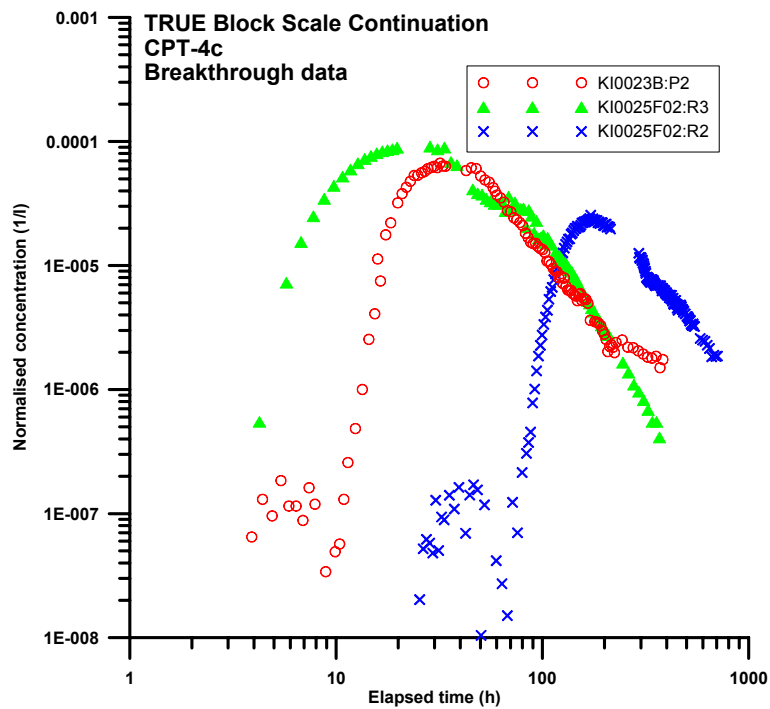


***Figure 3-19.*** *Tracer breakthrough curves for test CPT-4b, injection in KI0025F02:R2 (blue), KA2563A:S1 (green) and KA2563A:S2 (red), logarithmic time scale. Concentrations are normalised to injected mass.*

In CPT-4c breakthrough was showed in all three sections, cf. Figure 3-20 and 3-21. The lack of data in the graphs is due to problems with the automatic sampler.



*Figure 3-20.* *Tracer breakthrough curves for test CPT-4c, injection in KI0023B:P2( red), KI0025F02:R3 (green) and KI0025F02:R2 (blue), linear time scale. Concentrations are normalised to injected mass.*



*Figure 3-2.* *Tracer breakthrough curves for test CPT-4c, injection in KI0023B:P2 (red), KI0025F02:R3 (green) and KI0025F02:R2 (blue), logarithmic time scale. Concentrations are normalised to injected mass.*

Tracer mass recovery, presented in Table 3-7, was calculated by integrating the breakthrough curves for mass flux (mg/h) versus time (h) in the pumping borehole section. The injected mass was calculated by weighing the tracer solution vessel during the injection procedure.

**Table 3-7. Tracer mass recovery in pumping section KI0025F03:R3 during test CPT-4a to CPT-4c.**

| Inj. section | Structure | Tracer | Recovery (%) | Sampling time (h) |
|---|---|---|---|---|
| **CPT-4a** | | | | |
| KI0025F:R2 | #19 | Rhodamine WT | 41 | 716 |
| KI0025F02:R3 | #19 | Amino G Acid | 79 | 701 |
| KI0023B:P2 | #19 | Uranine | 124 | 718 |
| **CPT-4b** | | | | |
| KA2563A:S1 | #19 | Uranine | 78 | 1721 |
| KA2563A:S2 | #19 | Rhodamine WT | 3 | 1718 |
| KI0025F02:R2 | #25 | Amino G Acid | 79 | 167 |
| **CPT-4c** | | | | |
| KI0025F02:R3 | #19 | Uranine | 84 | 369 |
| KI0023B:P2 | #19 | Rhodamine WT | 65 | 384 |
| KI0025F02:R2 | #25 | Amino G Acid | 80 | 706 |

## 3.6   Supporting data

The head distribution in Structures #19 and #25 during the entire test period are shown in Figure 3-22. The influence of the pumping in different sections are clearly seen, see also Log of Events in Table 3-1. A slowly decreasing pressure trend in the sink, KI0025F03:R3, is also clearly seen indicating restrictions in the flow system (i.e. a no-flow boundary). The low pressure in section KI0025F02:R2 in January 2004 is due to a water sampling campaign. Comments on the pressure- and concentration data from test CPT-1-CPT-4 are presented below.

CPT-1

Pressure disturbance from water sampling in borehole KA2563A:S4 030918 08:00-030918 09:42 and water sampling in the Prototype Repository.

The activities have also affected many other borehole sections in KI0025F, KI0025F02, KI0025F03 and KI0023B.

CPT-2

Major pressure disturbance from drilling of borehole KA1619A01 at the 220 m level disturbing all pressures from 030924 08:00 until the end of the test.

Data loss in boreholes KI0025F, KI0025F02, KI0025F03, KI0023B and KA3510A from 030923 11:36:36 until 030924 08:21:18 due to major power failure in southern Sweden.

CPT-3

Pressure disturbance from open borehole KA1619A01 but stable pressures from start of pumping 030930 08:30:00 until 031001 14:47:00 when the borehole is closed. This affects all boreholes.

CPT-4

A pump failure occurred in test CPT-4b, injection in KI0025F02:R2 between November 28th 15:00 and December 2nd 10:30. This gives a distinct effect on the breakthrough curve.

Injection data for KI0025F02:R2 during CPT-4c is quite noisy due to a very low circulation rate which gave an uneven distribution of the tracer solution during the 7 hour long injection procedure.
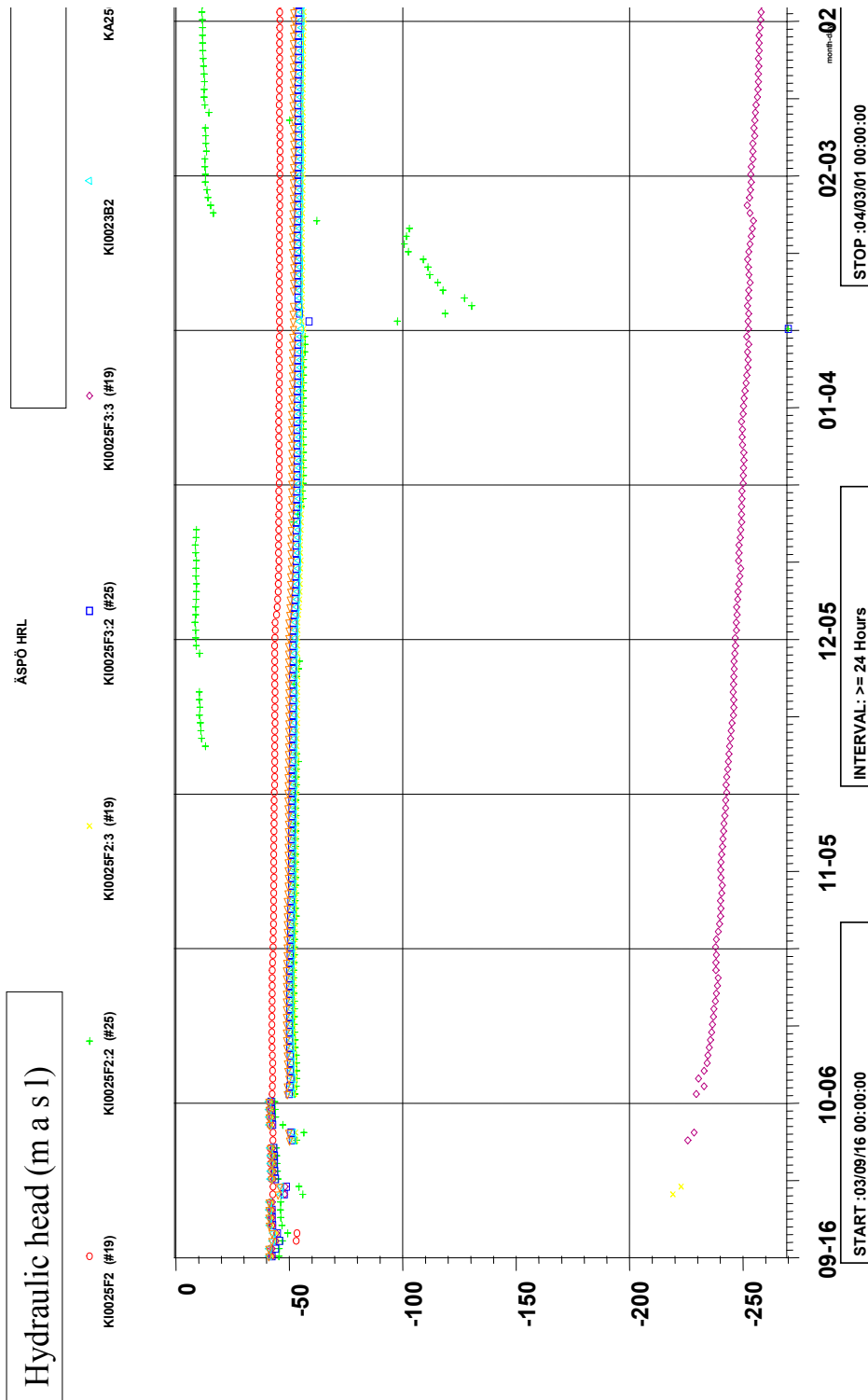
*Figure 3-22. Hydraulic head in Structures #19and #25 during TRUE Block Scale Continuation pre-tests CPT-1 - CPT-4.*

# 4 Model evaluation of tracer breakthrough

## 4.1 Estimation parameters and overall results

The following parameters were estimated for each model:

- AD-1: $v$ (average water velocity), $a_L$ (longitudinal dispersivity), $pf$ (proportionality factor)

- AD-2: $v_1, a_{L,1}, pf_1$ (pathway 1); $v_2, a_{L,2}, pf_2$ (pathway 2)

- MD: $v, a_L, pf, A$ (matrix diffusion parameter)

As was mentioned earlier in Chapter 2.4.1, the parameter $pf$ also represents dilution effects in the sampling section. Thus, this parameter may be included in the model fitting even if only one transport path is considered. For a single transport pathway and when the function $C_0(t)$ (injection concentration) is known, $pf$ may be expressed as:

$$pf = \frac{Q_{inj}}{Q_w} \cdot \text{loss factor} \tag{4-1}$$

where $Q_{in}$ is the flow rate leaving the injection section and $Q_w$ is the pumping flow rate in the sampling section.

The function $C_0(t)$ is often known only with large uncertainties. In addition, the parameter $pf$ may also be used to account for miscellaneous proportional losses such as sorption of tracer on equipment. Thus, the parameter $pf$ should be regarded as a composite parameter accounting for dilution, uncertainty in tracer injection, other proportional tracer losses, and, in the cases of more than one transport pathway, also as a distribution factor for each pathway.

In the next sections, the model evaluation of each tracer breakthrough curve is presented together with a few comments about each model fit. All estimated parameter values and estimation standard errors (in percent of estimated value) are compiled in Table 4-1.

**Table 4-1. Summary of estimated parameter values (estimation standard errors in percent of estimated value are given in parentheses)**

| | Model | AD-1 | | | AD-2 | | | | | | MD | | | |
|---|---|---|---|---|---|---|---|---|---|---|---|---|---|---|
| | Parameter | $t_0$ | $a_L$ | pf | $t_{01}$ | $a_{L1}$ | $pf_1$ | $t_{02}$ | $a_{L2}$ | $Pf_2$ | $t_0$ | $a_L$ | Pf | A |
| | Units | hour | m | - | hour | m | - | hour | m | - | hour | m | - | $s^{\frac{1}{2}}$ |
| **#** | **Tracer** | | | | | | | | | | | | | |
| **4 a** | RdWT | 148 (1.1) | 23.3 (3.9) | $2.04 \times 10^{-4}$ (1.1) | 97.6 (1.2) | 5.59 (27) | $8.64 \times 10^{-5}$ (42) | 234 (25) | 22.6 (73) | $1.35 \times 10^{-4}$ (28) | 80.9 (4.9) | 4.73 (11) | $2.79 \times 10^{-4}$ (1.2) | 448 (7.8) |
| | Amino G | 13.4 (1.6) | 13.0 (7.0) | $2.69 \times 10^{-4}$ (0.8) | - | - | - | - | - | - | 15.3 (12) | 6.57 (18) | $2.95 \times 10^{-4}$ (1.7) | 511 (28.2) |
| | Uranine | 38.4 (1.8) | 3.78 (10) | $1.25 \times 10^{-4}$ (1.6) | 35.3 (1.1) | 2.50 (6.2) | $1.14 \times 10^{-4}$ (1.4) | 43.0 (15) | 4.63 (41) | $4.52 \times 10^{-5}$ (25) | 19.9 (3.6) | 0.11 (73) | $1.48 \times 10^{-4}$ (1.2) | 261 (7.2) |
| **4 b** | RdWT | 751 (1.0) | 2.24 (6.7) | $7.12 \times 10^{-2}$ (2.8) | - | - | - | - | - | - | - | - | - | - |
| | Amino G | 178 (0.7) | 6.41 (2.7) | $4.39 \times 10^{-4}$ (0.8) | - | - | - | - | - | - | 174 (6.7) | 3.92 (11) | $5.20 \times 10^{-4}$ (2.7) | 1682 (23) |
| | Uranine | 361 (1.3) | 8.45 (6.8) | $1.01 \times 10^{-4}$ (1.5) | 736 (38) | 60.7 (30) | $7.78 \times 10^{-5}$ (21) | 334 (1.4) | 3.11 (18) | $5.70 \times 10^{-5}$ (13) | 279 (8.8) | 3.47 (22) | $1.32 \times 10^{-4}$ (4.1) | 1372 (23) |
| **4 c** | RdWT | 29.5 (1.2) | 3.83 (6.2) | $8.47 \times 10^{-4}$ (1.8) | 25.9 (2.4) | 2.22 (9.9) | $6.32 \times 10^{-4}$ (20) | 78.4 (34) | 9.24 (121) | $3.78 \times 10^{-4}$ (38) | 17.9 (3.6) | 0.89 (12) | $1.22 \times 10^{-3}$ (1.4) | 234 (7.1) |
| | Amino G | 209 (0.5) | 1.81 (2.4) | $5.74 \times 10^{-4}$ (1.1) | 190 (1.5) | 1.27 (3.3) | $4.56 \times 10^{-4}$ (4.3) | 437 (3.6) | 1.42 (29) | $1.73 \times 10^{-4}$ (14) | 142 (1.5) | 0.80 (4.0) | $7.77 \times 10^{-4}$ (4.7) | 1032 (4.7) |
| | Uranine | 11.1 (2.9) | 5.29 (15) | $1.44 \times 10^{-3}$ (2.3) | 10.2 (4.8) | 2.94 (29) | $1.10 \times 10^{-3}$ (11) | 46.7 (105) | 111 (185) | $9.26 \times 10^{-4}$ (40) | 10.0 (14) | 2.71 (31) | $1.64 \times 10^{-3}$ (3.6) | 397 (41) |

Theoretical tracer recovery was evaluated for each of the model fits according to eq. 4-18 and is presented in Table 4.2. The tracer recovery values vary considerably but are in most cases acceptable. A very low recovery is obtained for CPT-4b (Rhodamine WT) because no circulation was possible and much of the injected mass was still in the injection system at the end of the test. A relatively low tracer recovery was also obtained from CPT-4A (Rhodamine WT). The test CPT-4a (Uranine) resulted in very high tracer recovery that possibly indicates some tracer analysis error, cf Chapter 3.5.

**Table 4-2. Theoretical tracer mass recovery calculated from the model fits.**

| Test | Tracer | Model | Recovery (%) |
|---|---|---|---|
| CPT-4a | Rhodamine WT | AD-1 | 41.1 |
| | | AD-2 | 44.8 |
| | | MD | 49.4 |
| CPT-4a | Amino G Acid | AD-1 | 76.7 |
| | | AD-2 | - |
| | | MD | 82.6 |
| CPT-4a | Uranine | AD-1 | 110.3 |
| | | AD-2 | 140.5 |
| | | MD | 124.1 |
| CPT-4b | Rhodamine WT | AD-1 | 9.1 |
| | | AD-2 | - |
| | | MD | - |
| CPT-4b | Amino G Acid | AD-1 | 76.7 |
| | | AD-2 | - |
| | | MD | 84.1 |
| CPT-4b | Uranine | AD-1 | 73.7 |
| | | AD-2 | 127.8 |
| | | MD | 81.4 |
| CPT-4c | Rhodamine WT | AD-1 | 52.2 |
| | | AD-2 | 62.2 |
| | | MD | 71.1 |
| CPT-4c | Amino G Acid | AD-1 | 74.0 |
| | | AD-2 | 81.1 |
| | | MD | 89.5 |
| CPT-4c | Uranine | AD-1 | 70.6 |
| | | AD-2 | 98.7 |
| | | **MD** | 79.1 |

## 4.2    Test CPT-4A

### 4.2.1    Rhodamine WT

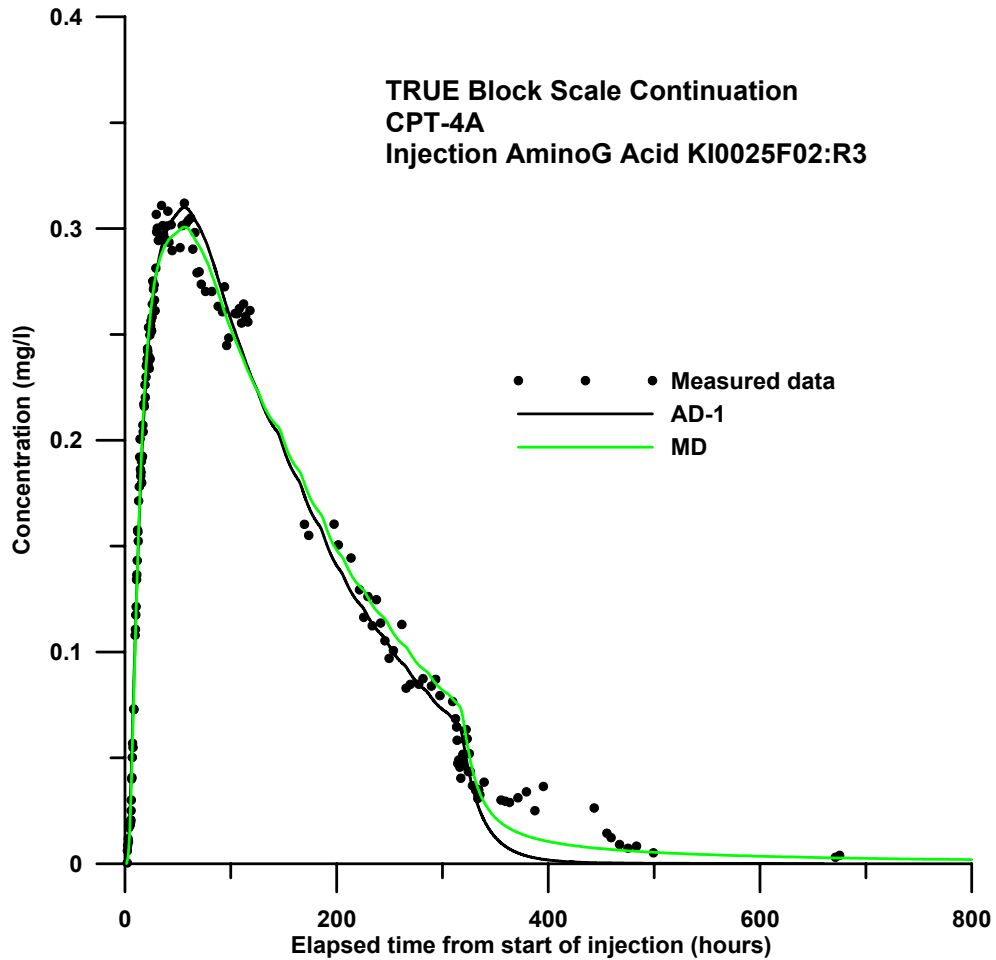The injection source/structure is KI0025F:R2/# 19 and the best-fit model evaluation is shown in Figure 4-1.
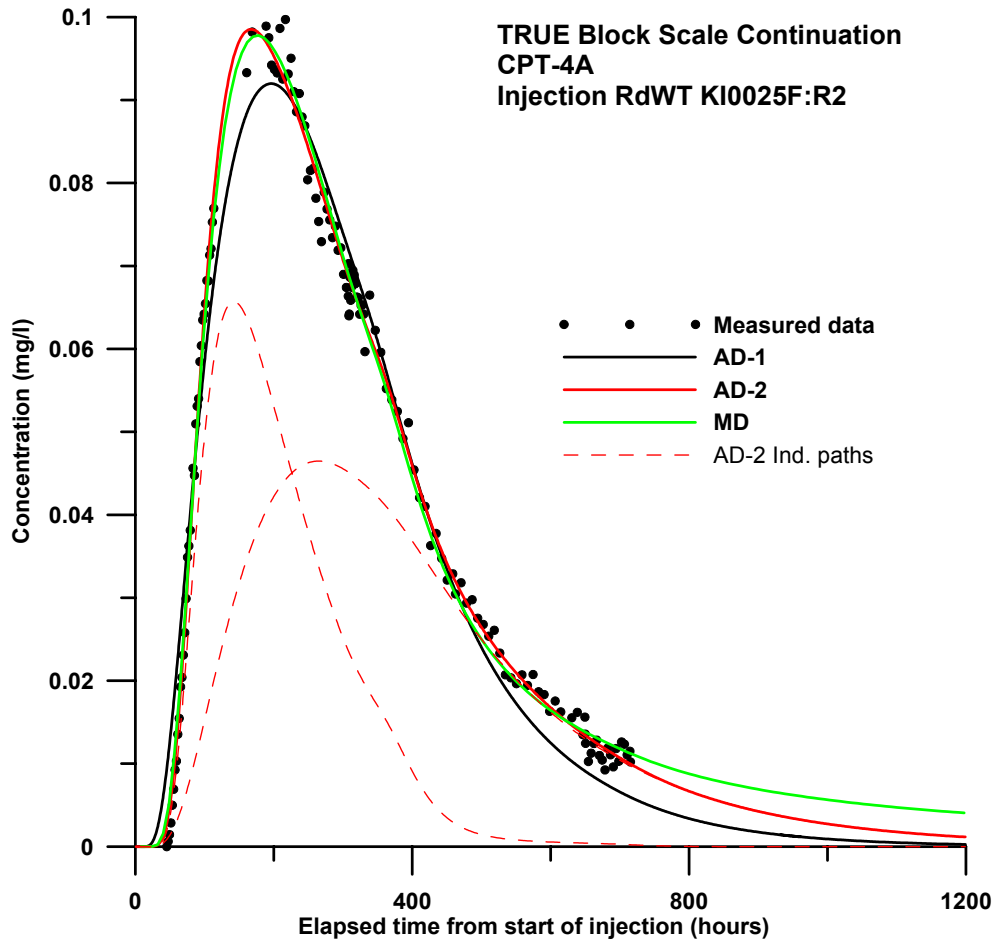


*Figure 4-1.* *Model fitting of Rhodamine WT breakthrough in test 4a.*

Comments:

- Both the AD-2 and MD models give somewhat better model fit than AD-1

- Estimated parameter values are within expected limits; moderately high estimation errors for the AD-2 model, small estimation errors for the AD-1 and MD models

- Theoretical recovery is about 45 % for the AD-2 model and about 49 % for the MD model. This is in good agreement with the measured value of 41 % at 700 hours of elapsed time.

## 4.2.2 Amino G Acid

The injection source/structure is KI0025F02:R3/# 19 and the best-fit model evaluation is shown in Figure 4-2.



*Figure 4-2. Model fitting of Amino G Acid breakthrough in test 4a.*

Comments:

- Both the AD-1 and MD models result in similar fits; unexplained increase in breakthrough curve at about 400 hours

- Estimated parameter values are within expected limits; small estimation errors

- Theoretical recovery is about 77 % for the AD-1 model and about 83 % for the MD model

### 4.2.3 Uranine

The injection source/structure is KI0023B:P2/# 19 and the best-fit model evaluation is shown in Figure 4-3.
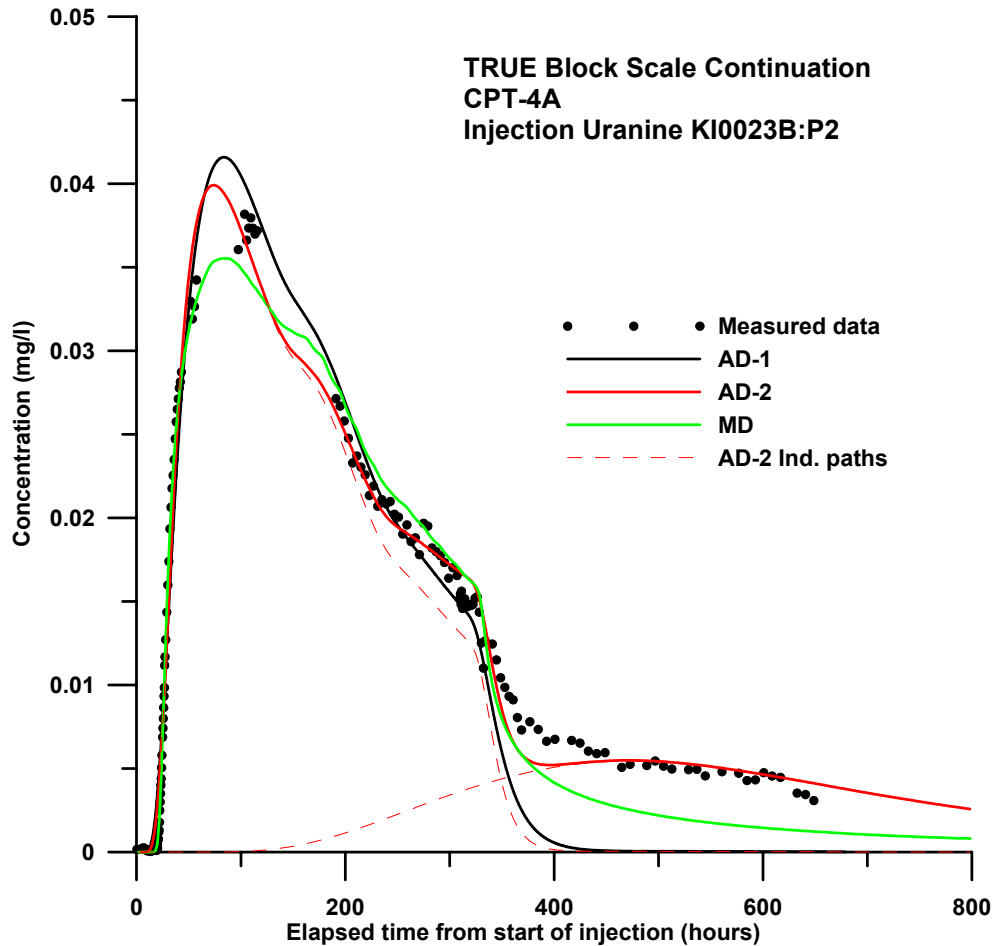


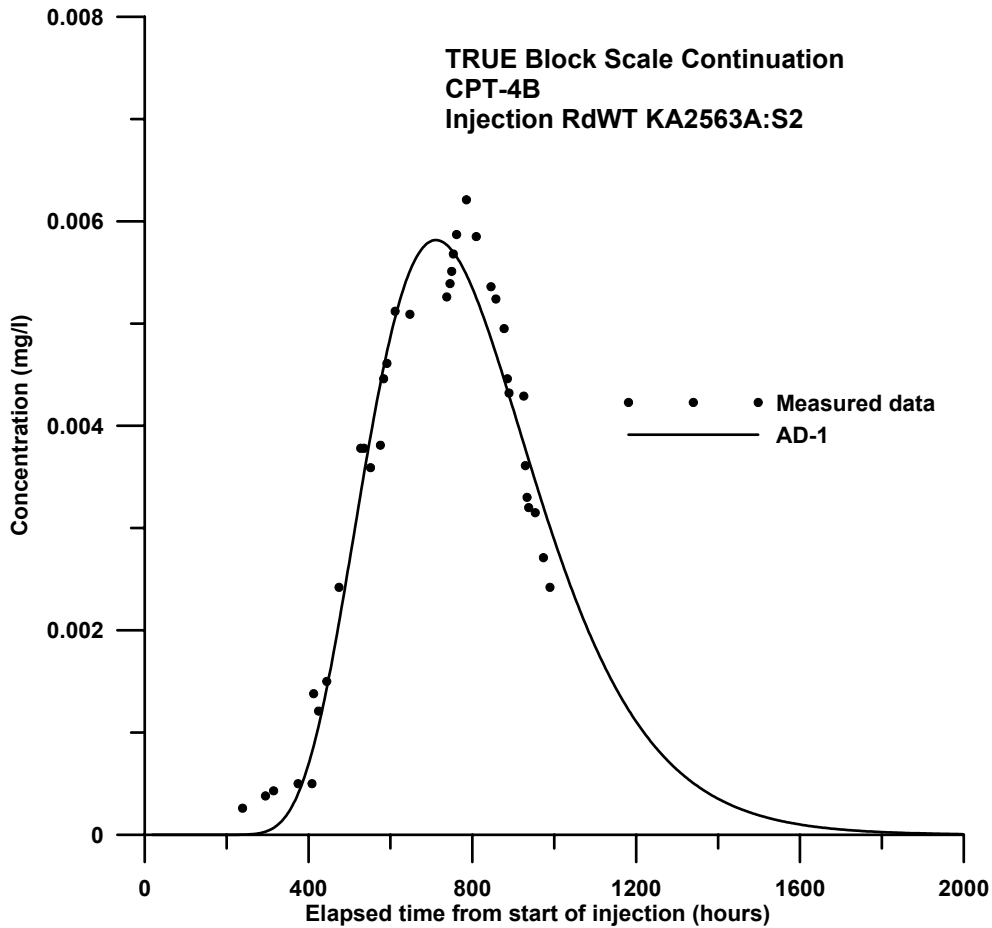*Figure 4-3. Model fitting of Uranine breakthrough in test 4a.*

Comments:

- None of the models result in entirely satisfactory fits at the end of the breakthrough curve; the AD-1 model clearly gives the worst fit

- Estimated parameter values are within expected limits, except for the MD model which results in a dispersivity value of 0.11 m; generally small estimation errors

- Recovery calculations give unusually high values and indicate possible errors in the measured breakthrough concentrations; the theoretical recovery for the AD-2 model is about 140 % and about 124 % for the MD model

## 4.3    Test CPT-4B

### 4.3.1    Rhodamine WT

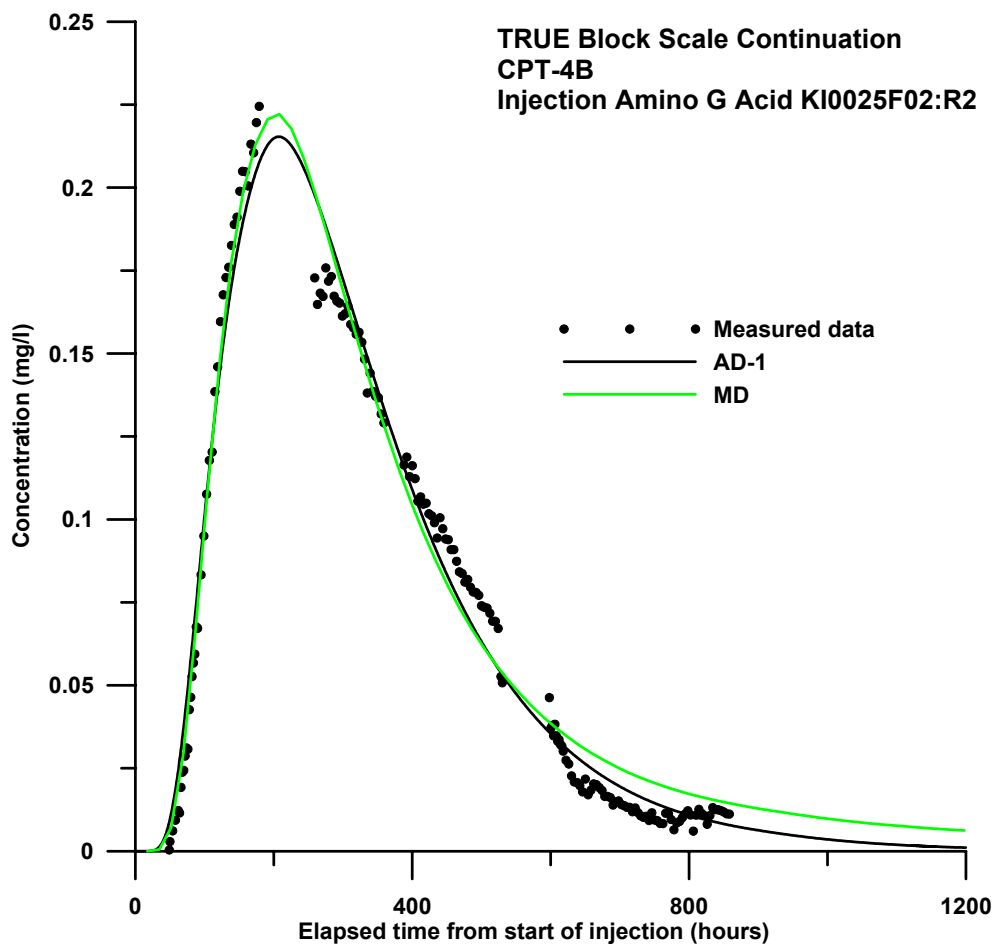The injection source/structure is KA2563A:S1/# 19 and the best-fit model evaluation is shown in Figure 4-4.



***Figure 4-4.*** *Model fitting of Rhodamine WT breakthrough in test 4b.*

Comments:

- Only the AD-1 model is fitted because of sparse data and missing breakthrough curve tail

- Estimated parameter values are within expected limits; small estimation errors

- Theoretical recovery is only about 9.0 %. The explanation for this low result is likely connected to the anomalous injection conditions during this test

61

### 4.3.2   Amino G Acid

The injection source/structure is KI0025F02:R2/# 25 and the best-fit model evaluation is shown in Figure 4-5. During this experiment, a pump failure occurred which results a clear disturbance in the experimental breakthrough curve. Therefore, both the original injection data as well as the original tracer breakthrough data have been adjusted in order to approximately account for the effects of the pump failure. The adjustment consists of deleting and adjusting (in time) data in such a way that the pump failure period is eliminated altogether. This is clearly a very approximate way of accounting for the pump failure, and the results from the model evaluation should thus also be considered relatively uncertain.



*Figure 4-5. Model fitting of Amino G Acid breakthrough (adjusted for pump failure between November 28 (15:00) and December 2 (10:30)) in test 4b.*
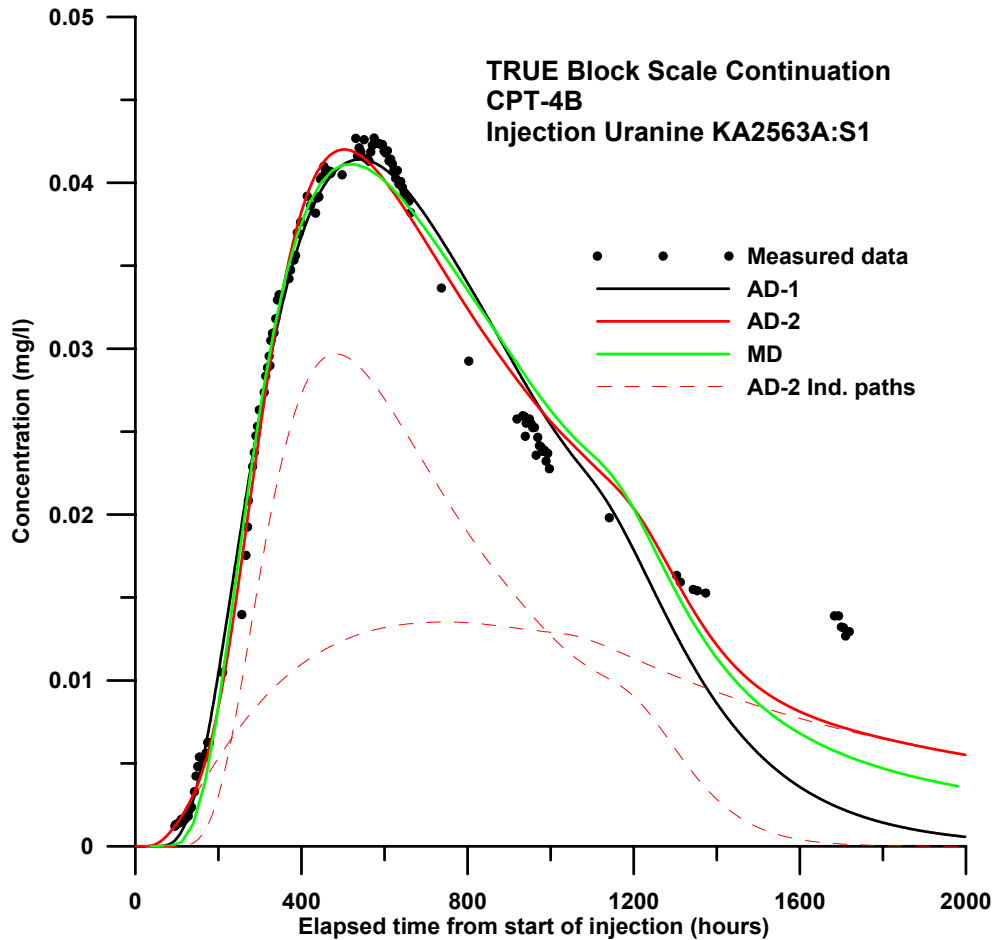
Comments:

- Both the AD-1 ands MD models result in reasonable good fits, given the added uncertainties from the pump failure

- Estimated parameter values are within expected limits; small estimation errors

- Theoretical recovery is about 77 % for the AD-1 model and about 85 % for the MD model

### 4.3.3    Uranine

The injection source/structure is KA2563A:S1/# 19 and the best-fit model evaluation is shown in Figure 4-6.



**Figure 4-6.** *Model fitting of Uranine breakthrough in test 4b.*

Comments:

- All models fit reasonably well to the breakthrough data, except at the end of the curve. At the end of the curve, the AD-2 and MD models is somewhat better than the AD-1 model, but still not explaining the relatively high concentration values for the last few measurement points

- Estimated parameter values are within expected limits, except for an excessively high dispersivity value (60.7 m) for the second pathway in the AD-2 model; estimation errors are generally small (AD-1 and MD models) to moderate (AD-2 model)

- The theoretical recovery is about 127 % for the AD-2 model and about 81 % for the MD model.

## 4.4    Test CPT-4C

### 4.4.1    Rhodamine WT

The injection source/structure is KI0023B:P2/# 19 and the best-fit model evaluation is shown in Figure 4-7.
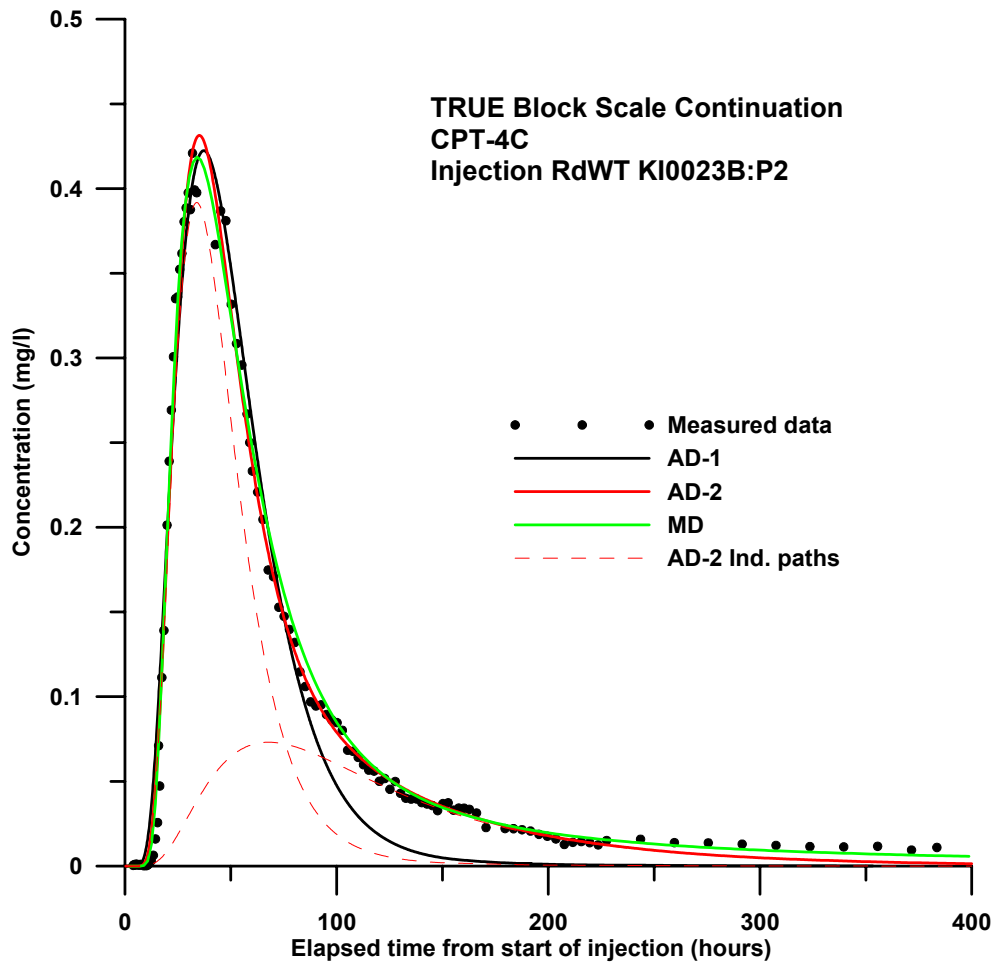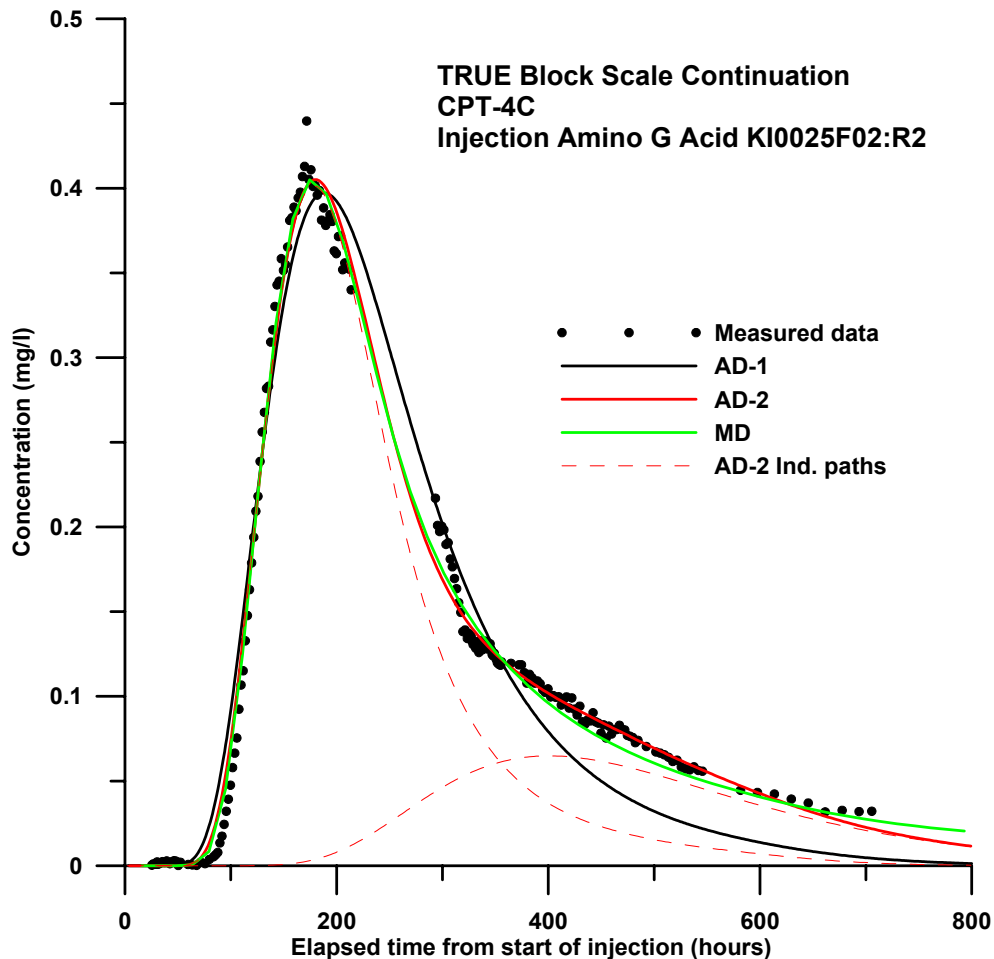


*Figure 4-7. Model fitting of Rhodamine WT breakthrough in test 4c.*

Comments:

- Better fits for the AD-2 and MD models than for the AD-1 model. Further, the MD model fits the tail slightly better than the AD-2 model.

- Estimated parameter values are within expected limits; estimation errors are generally small for the AD-1 and MD models but higher for the AD-2 model (an error of 121 % for the dispersivity value for the second pathway)

- The theoretical recovery is about 62 % for the AD-2 model and about 71 % for the MD model.

## 4.4.2 Amino G Acid

The injection source/structure is KI0025F02:R2/# 25 and the best-fit model evaluation is shown in Figure 4-8.



*Figure 4-8. Model fitting of Amino G Acid breakthrough in test 4c.*

Comments:

- Better fits for the AD-2 and MD models than for the AD-1 model. Further, the MD model fits the tail slightly better than the AD-2 model.

- Estimated parameter values are within expected limits; estimation errors are generally small for (AD-1 and MD models) to moderate (AD-2 model)

- The theoretical recovery is about 81 % for the AD-2 model and about 89 % for the MD model.

### 4.4.3 Uranine

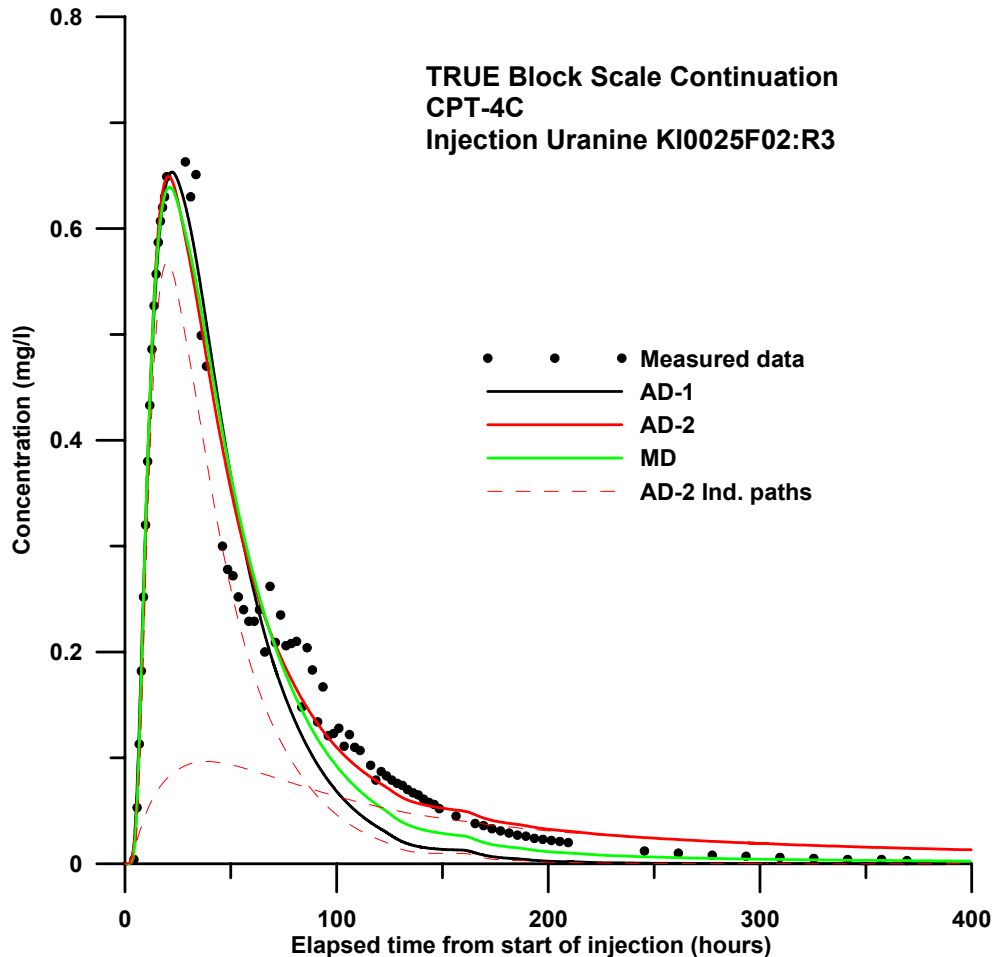The injection source/structure is KI0025F02:R3/# 19 and the best-fit model evaluation is shown in Figure 4-9.



*Figure 4-9. Model fitting of Uranine breakthrough in test 4c.*

Comments:

- Better fits for the AD-2 and MD models than for the AD-1 model. However, both of the latter two models fit indicate systematic errors during the descending and tail parts of the breakthrough curve.

- Estimated parameter values are within expected limits; estimation errors are generally small for the AD-1 model, moderate for the MD model, and relatively high for the AD-2 model

- The theoretical recovery is about 99 % for the AD-2 model and about 79 % for the MD model.

# 5 Discussion and conclusions

## 5.1 Connectivity and structural model

In general, the performed tests confirm the existing hydro-structural model (Winberg et al., 2002). The pressure interference tests CPT-1 to CPT-3, using Structure #19 as sink, show similar response patterns, with high and fast responses in sections interpreted to include Structure #19 and high but significantly slower responses in sections including Structure #25. Structure #20-system (Structure #20, #21, #22, #23) respond lower and slower.

There are only a few responses that do no follow the pattern described above, in particular the very good responses in sections KI00025F:R1 (Structure Z), KI0023B:P3, KI0025F:R3 and KI0025F03:R1. These responses indicate that other fractures connected to Structure #19 are present, possible splay fractures to Structure #19.

The determination of flow rates using the tracer dilution method was performed both under natural (ambient) gradient and during the pumping phases of tests CPT-1 to CPT-3. Each test included flow measurements of 7-8 sections and significant flow responses were noted during all three tests and in almost all sections measured. The magnitude of flow and flow responses are governed by the local transmissivity of the borehole section and the hydraulic gradient. Thus, natural (ambient) flow rates vary by between 3-42 ml/h and stressed flow rates go up as high as 400 ml/h due to the pumping (c.f. Tables 3-3 to 3-5).

The responses in test CPT-1 were less distinct than for the other tests except in KI0025F03:R3 where the response was significant (Table 3-3). Four sections show decreased flow while the rest show increased flow rates. This is consistent with the prevailing hydraulic gradient where sections located at an "up gradient" position in relation to the pumping section shows an increase in flow. A direction whereas section placed "down gradient" always shows a decrease in flow.

Tests CPT-2 and CPT-3 in Structure #19 generally show increased flow rates as the pumped section (KI0025F:R2) is located "down gradient" compared to Structure #19.

Section KI0025F03:R3 was judged to be the best sink for the tracer tests performed in CPT-4 due to good flow and pressure responses, central location and suitable distance.

The general conclusion drawn from the results of the pressure interference tests and tracer dilution tests is that the TRUE Block Scale array consists of at least three well separated hydraulic units, Structure #19, Structure #25 and Structure #20. The tracer tests in CPT-4 show that Structure #19 and Structure #25 are interconnected since the mass recovery in KI0025F02:R2 was 80% in CPT-4b and 65% in CPT-4c. However, the implementation of the new structure #25 is questionable as it seem to consist of two separate fractures, only being indirectly connected through Structure #19.

The main objective with the CPT-4 pre-tests was to obtain further information of the test geometry proposed for the radioactive sorbing tracer tests planned within the TRUE Block Scale Continuation project. Based on the results of the CPT-4 experiments (and the limitation that injections can only be performed in flow paths where a recovery >80% has been proven from the permit from SSI), two different types of flow paths could be foreseen for tracer injection with sorbing tracers:

- Transport in a single structure (#19). The only potential flow path having a mass recovery of > 80% is KI0025F02:R3 → KI0025F03:R3.

- Tracer transport involving a single background fracture (#25) in contact with structure #19. The only flow path available for a tracer experiment addressing this type of transport is the KI0025F02:R2 → KI0025F03:R3 flow path. This flow path has also given a mass recovery of > 80%.

## 5.2    Transport and evaluated parameters

The model fits are generally fairly good for all of the nine breakthrough curves. In most of the cases, the AD-1 model (Advection-Dispersion, single flow path) appears to be inadequate for explaining the later parts of the curves, while the AD-2 (Advection-Dispersion, two flow paths) and MD (Advection-Dispersion-Matrix diffusion, single flow path) models in those cases usually provide a better fit. However, the AD-2 and MD models in many cases also show systematic model errors in the later parts of the curves. In three of the curves (Uranine and Amino G Acid in CPT-4A; Uranine in CPT-4B), high concentrations remain at later parts of the curve that neither the AD-2 model nor the MD model can reproduce.

Generally, estimated values are within typical ranges what may be expected for tracer tests on this scale. In only a few cases, parameter values appear to be unreasonably large or small. Estimation errors, as expressed by the standard error defined in Chapter 2.4.1, are also relatively small. In a few cases, large estimation errors occur, usually when the AD-2 model is applied. This is not surprising, since the AD-2 model contains a relatively large number (six) of parameters which often would be expected to result in larger standard errors than for models with fewer parameters.

Estimated values of the tracer residence time range between about ten hours, for the faster transport pathways, to several hundreds of hours for the slower pathways. The estimated values of the dispersivity are typically in the range of a few metres, except for some of the pathways from fits with the AD-2 model. The parameter $A$ may be regarded as an approximate measure of the "effect" of matrix diffusion. This parameter is a composite measure of several more basic properties, such as rock porosity, diffusivity, etc (see eq. 4-11). In order to make any conclusions about the basic properties contained in the $A$ parameter, additional data would be required. The estimated values of $A$ are consistent with typical ones obtained from other experiments in fractured crystalline rock (Moreno et al, 1983, Andersson et al, 2002b).

In the cases where more than one model fits the data well, there are only limited possibilities to discriminate between the models, i.e. make judgements about which model is "best". In some instances, estimated parameter values are clearly out of the characteristic range of typical values. Unambiguous identification of matrix diffusion processes generally requires simultaneous injection of two or more tracers with different diffusivities and, thus, no definite conclusions about matrix diffusion effects may be made from theses tests.

In three of the performed tests, the test geometry was identical and the results may then be compared more directly. The pairs of tests that can be compared are listed in Table 5.1.

**Table 5-1. Pairs of tests performed in the same test geometry.**

| Test/tracers | | Source/structure |
|---|---|---|
| CPT-4a/Amino G Acid | CPT-4c/Uranine | **KI0025F02:R3/#19** |
| CPT-4a/Uranine | CPT-4c/Rhodamine WT | **KI0023B:P2/#19** |
| **CPT-4b/Amino G Acid** | **CPT-4c/Amino G Acid** | **KI0025F02/#25** |

The three pairs of tests that may be compared are commented on briefly as follows:

*CPT-4a/Amino G Acid - CPT-4c/Uranine*

The model fits for these tests are shown in Figures 4-2 and 4-9, respectively. A comparison of the travel times for the fitted models show that travel times are somewhat shorter for Uranine.

The test with Uranine in CPT-4c was performed with a small continuous injection of water (5.0 ml/min) and travel times would thus be expected to be shorter than for Amino G Acid in CPT-4a. Estimated dispersivity values are also smaller for Uranine, while the estimated values of the matrix diffusion parameter is of the same order for both tests. The breakthrough curve fits for both tracers are fairly good. However, in both cases there are measured concentrations towards the end of the breakthrough curves that are somewhat higher than any of the applied models is able to explain.

*CPT-4a/Uranine - CPT-4c/Rhodamine WT*

The model fits for these tests are shown in Figures 4-3 and 4-7, respectively. A comparison of the travel times for the fitted models show that travel times generally are somewhat shorter for Rhodamine WT. The test with Rhodamine WT in CPT-4c was performed with a small continuous injection of water (5.0 ml/min) and travel times would, thus, be expected to be shorter than for Amino Uranine in CPT-4a. Estimated values of dispersivity and the matrix diffusion parameter *A* do not indicate any clear differences between the tests. The breakthrough curve fit is clearly better for Rhodamine WT in test CPT-4c. The most significant difference is the unusually high concentrations that appear towards the end of the test with Uranine. This effect does not seem to occur at all in the corresponding test with Rhodamine WT in CPT-4c.

*CPT-4b/Amino G Acid  - CPT-4c/Amino G Acid*

The model fits for these tests are shown in Figures 4-5 and 4-8, respectively. Both of these tests were performed with a continuous injection of water, both at a flow rate of 2.0 ml/min, and should be expected to result in similar tracer breakthrough. However, because of the data adjustment (see above) due to a pump failure, a close comparison of results is probably not warranted in this case. Given the uncertainties in the data in this particular case, there appears to be a reasonable qualitative agreement between the results of these two tests.

# 6    References

**Andersson, P., Byegård, J., Dershowitz, B., Doe, T., Hermansson, J., Meier, P., Tullborg, E.-L.,Winberg, A.; 2002a:** Final report of the TRUE Block Scale project.1. Characterisation and model development. SKB Technical Report TR-02-13.

**Andersson, P., Byegård, J., Winberg, A.; 2002b:** Final report of the TRUE Block Scale project. Tracer tests in the block scale. SKB Technical Report TR-02-14.

**Andersson, P., Wass, E., Gröhn, S., Holmqvist, M., 2002c:** TRUE-1 Continuation project. Complementary investigations at the TRUE-1 site- Crosshole interference, dilution and tracer tests, CX-1 – CX-5. SKB International Progress Report IPR-02-47.

**Andersson, P., Ludvigson, J-E., Wass, E., Holmqvist, M., 2001:** TRUE Block Scale Detailed characterisation stage. Interference tests and tracer tests PT-1 – PT-4. SKB International Progress Report IPR-01-52.

**Cooley, R., L., 1979:** A method of estimating parameters and assessing reliability for models of steady state ground water flow. 2. Application of statistical analysis. Water Resources Research, 13: 603-617.

**Gustafsson E., Klockars C-E., 1981:** Studies of groundwater transport in fractured crystalline rock under controlled conditions using non-radioactive tracers. SKBF/KBS Technical Report TR 81-07.

**Javandel, I., Doughty, C., Tsang, C., F., 1984:** Groundwater transport: Handbook of mathematical models. American Geophysical Union, Water resources monograph series 10.

**Levenberg, K., 1944:** A method for the solution of certain nonlinear problems in least squares. Q. Appl. Math., 2: 164-168.

**Marquardt, D., W., 1963:** An algorithm for least squares estimation of non-linear parameters. J. Soc. Ind. Appl. Math. 11: 431-441.

**Moreno, L., Neretnieks, I., Klockars, C-E, 1983:** Evaluation of some tracer tests in the granitic rock at Finnsjön. SKBF/KBS Technical Report 83-38.

**Moreno, L., Neretnieks, I., Eriksen, T., 1985:** Analysis of some laboratory runs in natural fissures. Water Resources Research 21(7): 951-958.

**Moye D.G., 1967:** Diamond drilling for foundation exploration. Civil Eng. Trans., Inst. Eng. Australia (Apr. 1967), 95-100.

**Nordqvist R, 1994:** Documentation of some analytical flow and transport models implemented for use with PAREST - Users manual. GEOSIGMA Internal Report GRAP 94 006, Uppsala.

**Poteri, A., Billaux, D., Dershowitz, W., Gomez-Hernandez, J J., Cvetkovic, V., Hautojärvi, A., Holton, D., Medina, A., Winberg, A., 2002:** Final report of the TRUE Block Scale project. 3. Modelling of flow and transport. SKB Technical Report TR-02-15.

**Tang, D.H., Frind, E.O., Sudicky E.A., 1981:** Contaminant transport in fractured porous media: analytical solution for a single fracture. Water Resources Research 17(3): 555-564.

**Winberg, A., 1997:** Test plan for the TRUE Block Scale Experiment. SKB International Cooperation Report ICR 97-02.

**Winberg, A., Andersson, P., Poteri, A., Cvetkovic, V.Dershowitz, W., Hermanson, J., Gomez-Hernandez, J J., Hautojärvi, A., Billaux, D., Tullborg, E-L., Holton, D., Meier, P., Medina, A., 2002:** Final report of the TRUE Block Scale project. 4. Synthesis of flow,transport and retention in the block scale. SKB Technical Report TR-02-16.